METEOR-Berichte 02-2

North Atlantic 2001

Part 4

Cruise No. 50, Leg 4

17 July – 12 August 2001, Reykjavik – Hamburg

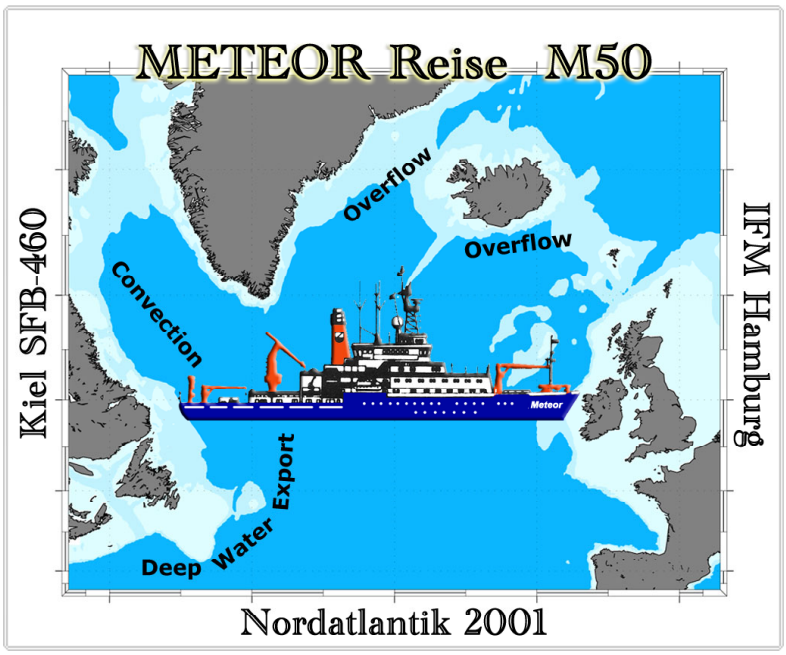

W. Zenk, J.D. Afghan, B. Bannert, M. Bleischwitz, K. Bulsiewicz, H. Cannaby, T. Csernok, U. Dombrowski, K. Friis, K. Fürhaupter, J. Greinert, J. Hauser, G. Karl, K. Lorbacher, H. Lüger, F. Malien, B. Marzeion, T. Müller, G. Niehus, M. Nielsen, W.-T. Ochsenhirt, J. Schafstall, R. Steinfeldt, T. Steinhoff

Editorial Assistance:

Frank Schmieder
Fachbereich Geowissenschaften, Universität Bremen

Leitstelle METEOR
Institut für Meereskunde der Universität Hamburg

2002

Table of Contents (M 50/4)

4.1 Participants of M50/4

1	Zenk, Walter, Dr.	Chief Scientist	IfMK
2	Afghan, Justine, D.	CO_2-Chemistry	IfMK/SIO
3	Bannert, Bernhard	UW Television	GEO/OKT
4	Bleischwitz, Marc	Tracer Physics	UBU
5	Bulsiewicz, Klaus	Tracer Physics	UBU
6	Cannaby, Heather	Coastal Oceanography Observer from Ireland	NUI
7	Csernok, Tiberiu	Marine Physics	IfMK
8	Dombrowsky, Uwe	Marine Physics	IfMK
9	Friis, Karsten, Dr.	CO_2-Chemistry	IfMK
10	Fürhaupter, Karin	Geochemistry	GEO/MaLi
11	Greinert, Jens, Dr.	Geochemistry	GEO
12	Hauser, Janko, Dr.	Oceanography	IfMK
13	Karl, Gerhard	Meteorology	DWD
14	Lorbacher, Katja, Dr.	Hydrography	BSH
15	Lüger, Heike	CO_2-Chemistry	IfMK
16	Malien, Frank	Marine Chemistry	IfMK
17	Marzeion, Benjamin	Marine Physics	IfMK
18	Müller, Thomas, Dr.	Marine Physics	IfMK
19	Niehus, Gerd	Marine Physics	IfMK
20	Nielsen, Martina	Marine Physics	IfMK
21	Ochsenhirt, Wolf-Thilo	Meteorology	DWD
22	Schafstall, Jens	Marine Physics	IfMK
23	Steinfeldt, Reiner	Tracer Physics	UBU
24	Steinhoff, Tobias	CO_2-Chemistry	IfMK

Participating Institutions

BSH Bundesamt für Seeschiffahrt und Hydrographie, Bernhard-Nocht-Str. 78, 20597 Hamburg – Germany, e-mail: koltermann@bsh.d400.de

DWD Deutscher Wetterdienst, Geschäftsfeld Schiffahrt, Bernhard-Nocht-Str. 76, 20359 Hamburg – Germany, e-mail: edmund.knuth@dwd.de

GEO Geomar Forschungszentrum für Marine Geowissenschaften, Wischhofstr. 1-3, 24148 Kiel – Germany, e-mail: rkeir@geomar.de

IfMK Institut für Meereskunde an der Universität Kiel, Düsternbrooker Weg 20, 24105 Kiel – Germany, e-mail: fschott@ifm.uni-kiel.de

MaLi MariLim, Büro für integrierte Meeres- und Küstenuntersuchungen, Wischhofstr. 1-3, Gebäude 11, 24148 Kiel – Germany, e-mail: tmeyer@marilim.de

NUI National University of Ireland, Newcastle Road, Galway - Republic of Ireland, e-mail: peter.bowyer@nuigalway.ie

OKT Oktopus, Gesellschaft für angewandte Wissenschaft, innovative Technologien und Service in der Meeresforschung mbH, Kieler Str. 51, 24594 Hohenwestedt – Germany, e-mail: schriever@biolab.com

SIO Scripps Institution of Oceanography, University of California, San Diego, 9599 Gilman Drive, La Jolla, CA 92093-0210 – USA, e-mail: jdafghan@pacbell.net

UBU Universität Bremen, Institut für Umweltphysik, Abt. Tracer-Ozeanographie, Bibliothekstraße, 28359 Bremen – Germany, e-mail: mrhein@physik.uni-bremen.de

4.2 Research Program

The fourth and last leg was again conducted by the *Institut für Meereskunde an der Universität Kiel*. SFB subproject A3 the revisited the Iceland Basin to continue measurements of the water mass variability in the subpolar gyre in the eastern basins of the North Atlantic. Research subjects are Labrador Sea Water penetrating from the west and Overflow Water entering from the northeast. Labrador Sea Water is generated annually by wintertime convection. Part of this water mass is advected eastward underneath the North Atlantic Current and over the Mid-Atlantic Ridge in the region of the Charlie Gibbs Fracture Zone at ~ 53°N. Its further penetration into the eastern basin is strongly influenced by mixing with Mediterranean Water, Subpolar Mode Water, and Overflow Water. Through these processes the low salinity tongue of Labrador Sea Water loses its prime characteristic properties while progressing northward into the Iceland Basin.

Water mass transformation processes also change the original properties of Iceland Scotland Overflow Water penetrating the Iceland Basin from the Norwegian Sea along the way southward. Then this partially mixed overflow water leaves the Iceland Basin for the Irminger Basin through gaps in the Reykjanes Ridge. Other diluted fractions follow the Mid-Atlantic Ridge as a deep western boundary current towards the Azores.

We aimed at making quantitative observations of transport fluctuations of the mentioned water masses. Such estimates are most relevant for the dynamics of the larger scale circulation of North Atlantic Deep Water. Modified Overflow Water, occasionally also called Charlie Gibbs Fracture Zone Water, is a main constituent of North Atlantic Deep Water. After leaving the subpolar gyre this water mass follows the continental slope of the Americas finally reaching the Antarctic Circumpolar Current. North Atlantic Deep Water is an integral limb of the global circulation and thus has a major impact on the global climate.

In cooperation with SFB subproject A1 moored equipment for monitoring the Denmark Strait Overflow Water had to be deployed during the beginning of the cruise. Like the Iceland Scotland Overflow, the Denmark Strait Overflow is another source for North Atlantic Deep Water.

Spreading paths of Labrador Sea and Overflow Waters in the Iceland Basin are subject to strong pulsations and shifts. These variations will be captured by eddy-resolving acoustically tracked RAFOS floats. Additional drifter launches support the newly initiated ARGO project.

The international ARGO Information Center has started to manage a sustained network of freely drifting ocean observing platforms. Their data are an essential part of future "ocean weather forecast". Within the next five years a fleet of 3000 deep sea drifters is planned. While drifting at 1500 m depth they cycle every ten days between 2000 m and the surface and transmit their data ashore. This information is broadcast via internet to operational oceanographers world wide within a day after the drifters reach the surfaces. The initial European contribution to ARGO is funded under GYROSCOPE by the European Commission in Brussels.

The return leg to Germany involved a repeat of WOCE section A2 between the Mid-Atlantic Ridge and the approaches of the European continent off Ireland. This work was conducted in co-operation with the Federal Maritime and Hydrographic Agency (BSH) in Hamburg. We completed the eastern part of A2 after its westward section had already been recorded during leg 1 in mid May 2001.

As part of the SFB project in Kiel the repeat hydrographic survey delivered chemical and tracer data with high vertical resolution and special consideration of pertinent CO_2 signals.

In addition, a group of geochemists from GEOMAR investigated methane sources. The latter were discovered during an earlier METEOR cruise at the Mid-Atlantic Ridge just south of Charlie Gibbs Fracture Zone. The group searched for the position and strength of a source in the region of the rift valley at 51°N and will determine the ratio of the stable carbon isotopes of the methane in its home laboratory in Kiel. In continuation of the geochemical water sampling the localizing of the sources was conducted by the Ocean Floor Observation System OFOS. It is hoped that the analysis phase will reveal the generation process (hydrodynamical smoker *versus* serpentination) in more detail.

4.3 Narrative of the Cruise

The majority of the scientific party arrived in Reykjavik on 16 July 2001. The day before the chief scientist Walter Zenk and a small group of technicians had taken over the ship from Jürgen Holfort and his team. Larger preparations of submersible gear were necessary for the sophisticated series of deep-sea moorings to be launched in Denmark Strait. The German ambassador to Iceland, Herr Dr Hendrik Dahne, visited METEOR twice while in port and arranged the visit of a team from the Icelandic National Television studios. As we were informed later by the embassy INT broadcast an extended report about the ship's mission on the day of departure.

On 17 July, 12:00, FS METEOR left Reykjavik and headed directly to the Denmark (or Greenland) Strait in good weather conditions and calm seas. On board were 24 scientists, technicians and students from eight institutions and companies plus two employees from the *Deutscher Wetterdienst (DWD).* Lists of personnel and contributing institutions are given in chapter 4.1, a list of stations in Table 4.3. After a transit of 27 hours we reached Sta. 307 on the afternoon of the next day. A cruise track chart is shown in Fig. 4.1.

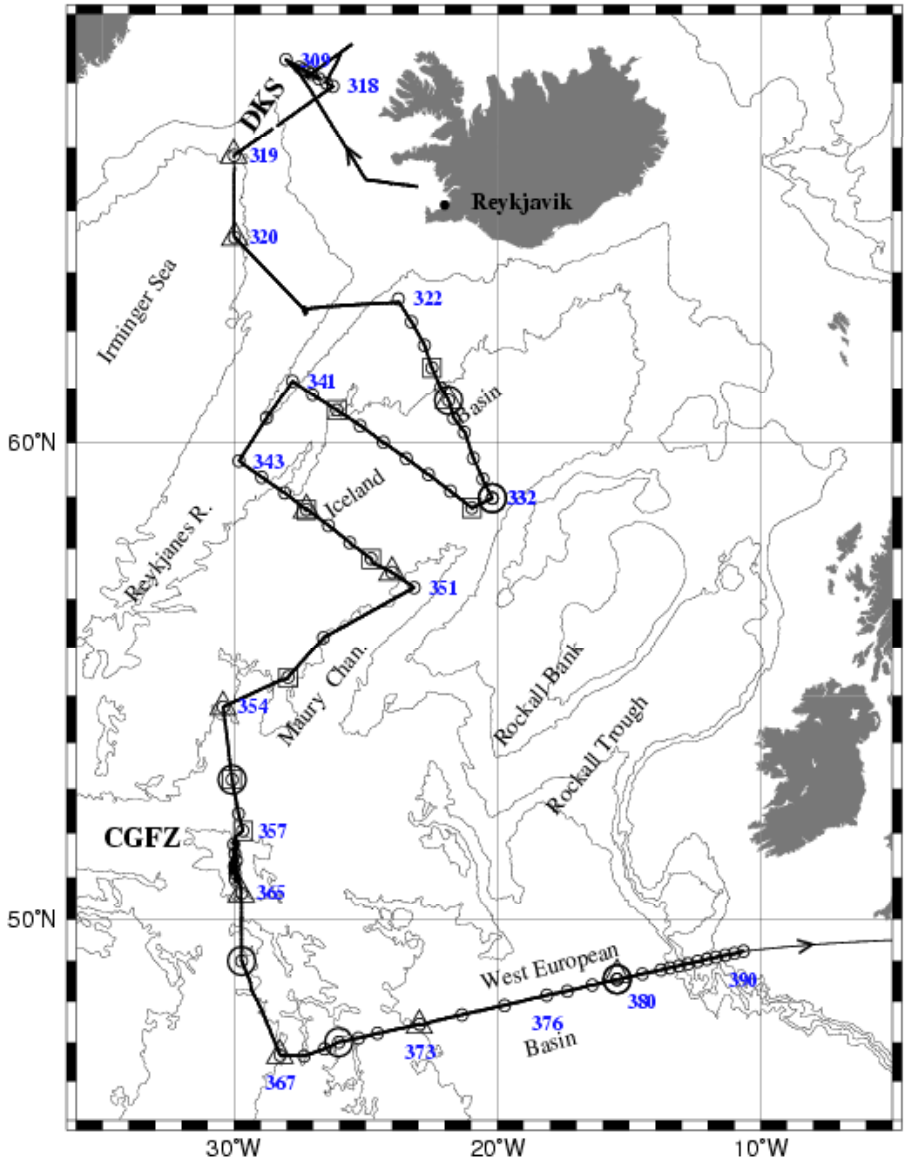

Fig. 4.1: Track chart METEOR cruise 50, leg 4. Legend: CTD stations (o), Thorium sites (O), APEX (triangles) & RAFOS launch sites (squares), Isobaths 1, 2, 3, 4 km.

We were pleased to find the site without ice and started primary functionality and handling trials with the **O**cean **F**loor **O**bservation **S**ystem (OFOS) and an acoustic release. This was a preparation exercise for the following deployment of the trawl resistant, remotely sensing current meter in the center of mooring gear V423_2 (SK). It comprises a hexagonal concrete shield housing and a modified **a**coustic **D**oppler **c**urrent **p**rofiling meter (ADCP). The device has been newly developed in Kiel to enable long-term observations of currents in bins of several hundred meters atop this near-bottom mooring. The test result was embarrassing because the auxiliary release for the joint deployment of the shielded ADCP and OFOS failed. It took several hours to reconstruct the OFOS frame for a spare release. Later in the evening we launched mooring V423 under permanent observation and documentation with the OFOS. We are sure to have it set on a flat bottom as confirmed by a short Hydrosweep survey prior to the station work.

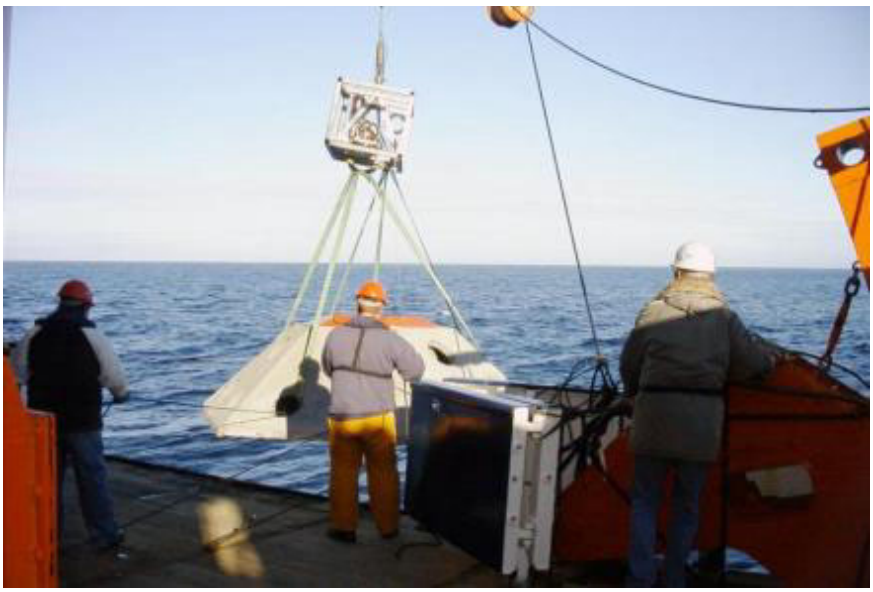

Fig 4.2: Deployment of shielded ADCP on Sta. 307.

Two additional moorings consisting of recording **P**ressure sensors and **I**nverted **E**cho **S**ounders (P/IES) were deployed on a section across the sill of Denmark Strait on Sta. 308 (Fig. 4.4) and 316. A final more conventional ADCP mooring without a shield was set on Sta. 315 in the deep out-flow channel where no fisheries activities are expected in contrast to the adjacent banks to both sites of the sill. All technical details on mooring work are summarized in Table 4.4. This table contains in its last row a remark on mooring V421_1 (TK). The latter was laid last summer by FS POSEIDON. While cautiously approaching the location on the afternoon of 19 July we realized that mooring TK apparently was situated just north of the closed ice margin as seen from our northern most position 66°34.5'N, 25°30.8'W. Hence, it was absolutely inaccessible for METEOR. Since more dense ice fields were drifting into the polar frontal region from the east (Fig 4.3), we were also unable to launch a prepared replacement mooring V421_2.

Without delay METEOR reversed its direction by 180°. We returned to the sill of Denmark Strait and supplemented the until then incomplete cross-sill CTD section (see inventory in Tab. 4.6) which includes lowered ADCP observations and regular water samples for analysis of numerous chemical substances including CFC, pCO_2, O_2 and nutrients. None of the ice barriers were forecast on the latest ices charts which we received from Greenland Command via IfM Kiel. After mid night of 19 July we had already settled the first phase of leg M50/4. The work load of the first phase was added relatively late in the planning stage of the expedition in due corse of the emergency case of FS POSEIDON. A multi-month long repair phase of this ship urged a complete revision of all IfM ship plans on which the field work of SFB 460 relies heavily.

Over the next few days the METEOR cruised southwestward into the Irminger Basin. There we launched two APEX drifters (see triangles in Fig 4.1). They are part of the internationally coordinated project ARGO. It aims at a future coverage of the world ocean with 3000 drifters for operational purposes. Our contribution at IfM Kiel is funded by the European Commission under GYROSCOPE. Initially METEOR carried ten APEX floats on board. Ten days later we received the first high quality up-cast CTD profiles from the first float cycles via satellite link from the CORIOLIS center in France.

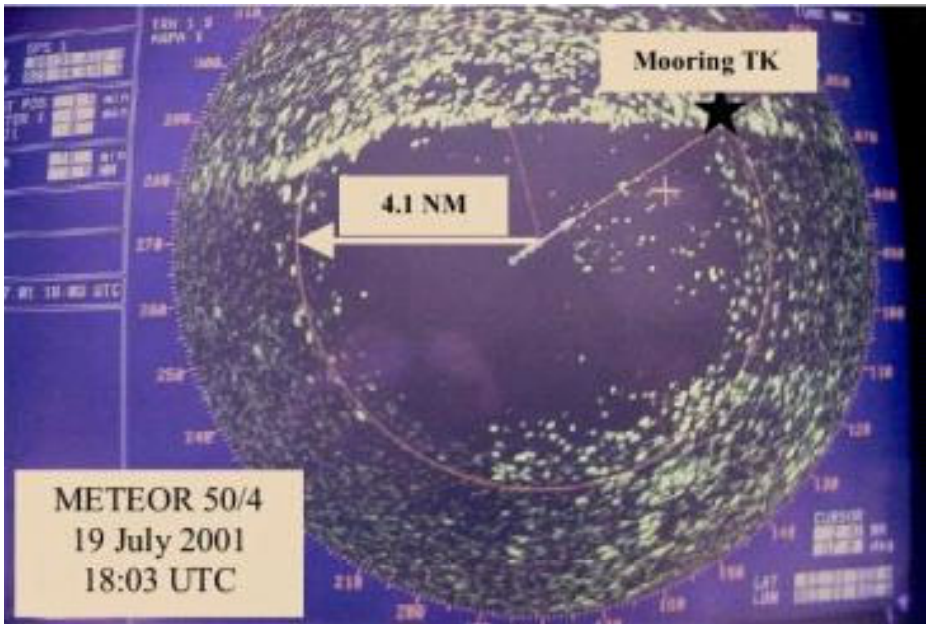

Fig. 4.3: Photograph of the icefield around mooring TK, taken from the radar screen of METEOR.

The second phase of M50/4 began on 21 July in the northern Iceland Basin after the vain search for a surfaced and transmitting RAFOS float on the Mid Atlantic Ridge (MAR) the day before. The sampling sites were targeted to cover CTD section **I** between the ridge and the more southeastward situated outskirts of Maury Channel, the deepest part of the Iceland Basin (Sta. 322-332). Station were located at near-by mooring positions which have been occupied since summer 2000. They were launched at strategic locations to monitor fluctuations of the Iceland Scotland Overflow entering the abyss of the Iceland Basin. Moorings along section **I** are planned for recovery in 2002.

Two more cross sections of the Iceland Basin were sampled (**A:** Sta. 333-341 and **B:** 343-351). In addition to APEX floats we launched eight eddy-resolving RAFOS floats in total (squares in Fig. 4.1). They are ballasted for the depth levels of the Labrador Sea Water (3 pieces) and the Overflow Water (5), respectively, and continue here and at more southerly situated positions earlier Lagrangian observations in the Iceland Basin (Davis & Zenk, 2001).

After repeat CTD/RO work north of Charlie Gibbs Fracture Zone (CGFZ) the remaining time was devoted to a detailed search for methane sources (Sta. 358-365) and to the subsequent repeat hydrographic section A2 of the **W**orld **O**cean **C**irculation **E**xperiment (WOCE). The core work of the GEOMAR group (see 4.4) on board concentrated on the meridionally oriented rift valley at 30°W south of the southern deep channel of the Fracture Zone. The expected occurrence of methane was confirmed at repeat and newly selected sampling sites. The 3-day sequence which included an intensive HYDROSWEEP survey of the valley, ended on 1 August with a 6 hour towed OFOS experiment showing excellent TV images from the eastern slope and the center of the rift valley.

After an additional station (366) for thorium samples METEOR reached the western end of the eastern half of WOCE A2. A series of full depth CTD stations with lowered ADCP obser-vations followed during the next five days. The 24 stations (367-390) were unevenly spaced with a more denser sampling on both sides of the crossed Western European Basin.

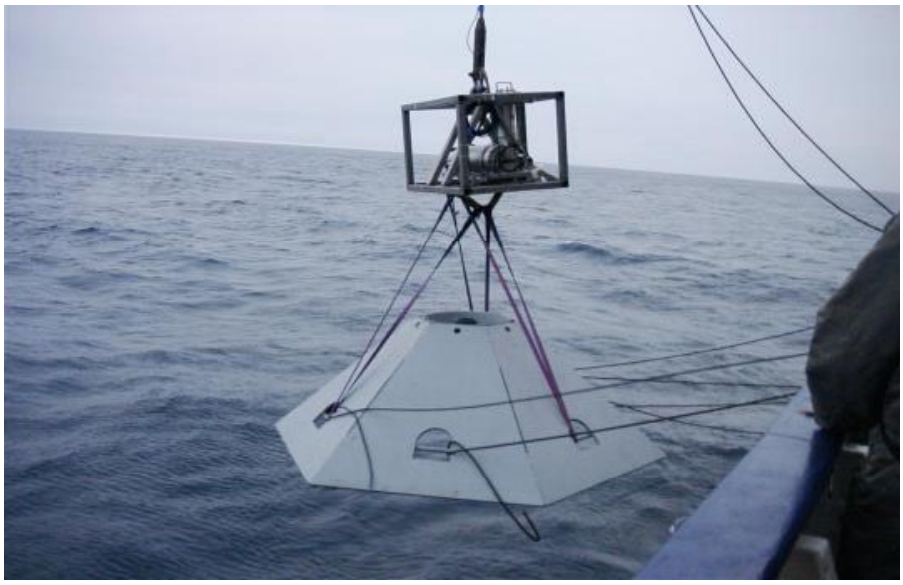

Fig. 4.4: Deployment of shielded echo sounder (P/IES06) by IfM Kiel in combination with video camera system OFOS (top) from GEOMAR.

The scientific work was terminated on 7 August at midnight and METEOR headed for her destination in Germany. We reached the shipyard in Rendsburg at noon on 12 August 2001.

4.4 Preliminary Results

4.4.1 Physical Oceanography

(J. Hauser, K. Lorbacher, F. Malien, T. J. Müller, W. Zenk)

Overview

The cruise covered a variety of different dynamic regimes of the northern North Atlantic. These can easily be distinguished by thermohaline records taken with the ship's thermosalinograph. In Fig. 4.5 we display sea surface temperature (T) and salinity (S). The diameters of the circles are proportional to the magnitudes of the parameters. We identify an arctic region that was covered at the beginning of the cruise. Temperatures dropped down to barely 0°C, the salinity decreased down to almost 31 at the ice edge. A subarctic region was crossed between the polar front in the Denmark Strait and the Reykjanes Ridge southwest of Iceland, marked by temperatures below and around 10°C. At ~52°N METEOR left the subpolar gyre and entered a domain with significantly warmer waters of mainly subtropical origin. The T/S data suggest a northward spreading of the North Atlantic Current focused and confined to the North by the Charlie Gibbs Fracture Zone. In the following paragraphs we present selected examples for the different oceanic regions as manifested in the hydrographic data. All profiles were collected by a Seabird CTD and 22 bottle rosette sampler. The CTD measurements were quality controlled onboard but not yet finally calibrated before arriving in Rendsburg.

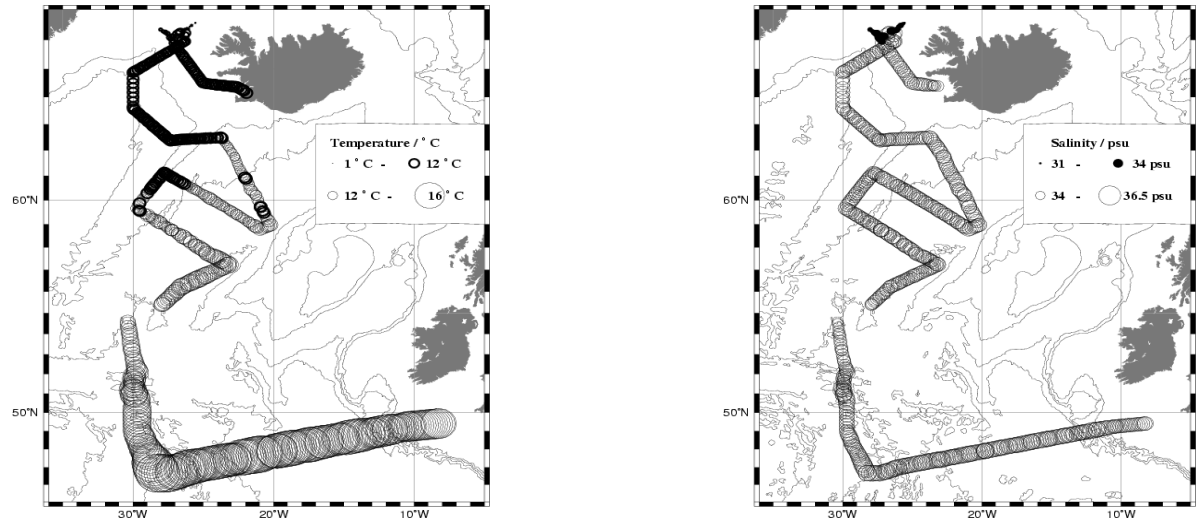

Fig. 4.5: Sea surface temperature (left) and salinity (right) from the ship mounted thermosalinograph. The diameter of the circles indicate magnitudes of the parameters.

CTD calibration and data processing

Temperature and pressure sensors

The CTD used on all stations on the cruise was a SeaBird 911 plus (internal IFM Kiel code SBE1) in conjunction with a SeaBird carousel. Due to external reasons, it was decided late in the planning phase for M50 that this instrument had to be the main one. Therefore, it had no fresh pre-cruise calibration for temperature and pressure sensors. However, during all stations, the pressure sensor read about –0.3 dbar (+/- 0.2 dbar) on deck immediately after a cast, indicating little drift, if any, in this sensor's calibration. As for the temperature sensor, experience with this type of sensor shows that it is stable also. Nevertheless, a post-cruise calibration of both sensors will be performed according to WOCE standards to allow for any significant corrections.

Salinity

The procedure was similar to that described by Müller (1999). Samples with rosette bottles were taken 20 m above the bottom, every 1000 dbar pressure levels and at 10 m depth. A Guildline AUTOSAL 8400B (internal IFMK code AS7) was standardized using standard seawater batch P137 (K15=0.99995, labelled S=34.998, ampoules filled December 1999). A drift of the salinomer's calibration of order 0.005 was confirmed independently by substandards taken from the deep sea and eliminated. This drift was not due to lab temperature which was recorded at 0.5 h intervals and was stable to within 0.2 K.

The resulting correction for the conductivity cell's output over leg M50/4 is linear in conductivity and time (cast). Recalculating salinity, the standard deviation of the residual SDIF is 0.0022 in salinity with most of the noise being associated with the 1000 dbar level where stratification is strong (cf. Fig. 4.6). In the deep sea of the eastern part of the WOCE section A2 the calibrated data match well the θ/S relation claimed to be stable by Saunders (1986) (Fig. 4.7).

As a secondary result note, that the ship-board thermosalinograph needs a salinity correction of 0.06 with standard deviation of 0.2 . No drift was obeserved here.

Processing

The CTD data were processed with the following steps (MÜLLER, 1999): range control; despiking; monotonizing with respect to inceasing pressure; minimum lowering velocity 0.2 dbar/s; median filter over 0.5 dbar intervals; interpolation to 0.5 dbar; calibration and recalculation of salinity; low pass cosine filter over 2.5 dbar; interpolation to 2 dbar. Later slight corrections for temperature and pressure sensor outputs will not affect salinity.

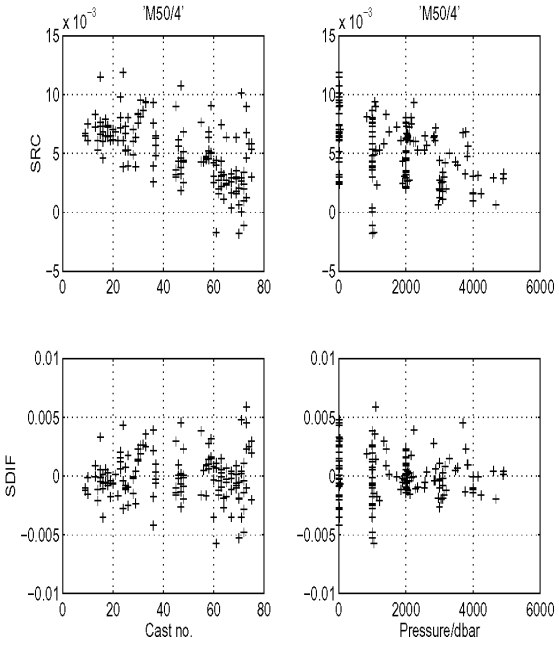

Fig. 4.6: Salinity correction for all CTD casts on cruise M50/4. Individual corrections SRC (upper panel) and residuals SDIF (lower panel) after calibration as functions of time (left: cast no.) and pressure (right). The standard deviation of the SDIF is 0.0022 in salinity.

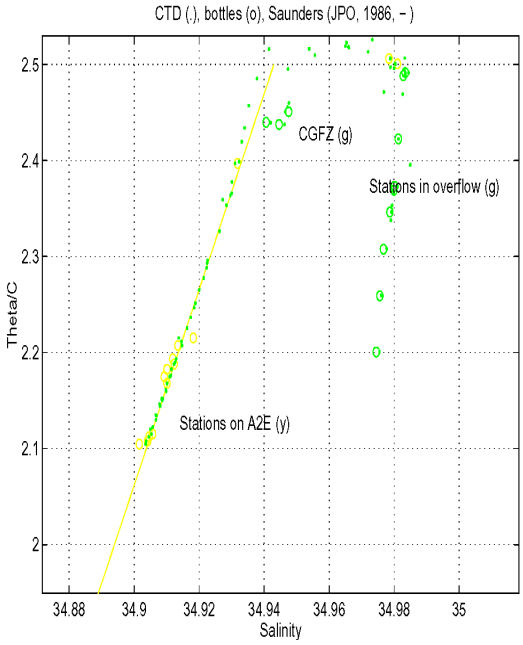

Fig. 4.7: Deep sea potential temperature/ salinity relation for all rosette samples (o) and CTD values (dots) at bottle depths. Three regimes appear clearly: Iceland Scotland overflow (ISOW) along the Reykjanes Ridge; CGFZ stations; eastern part of WOCE-section A2 stations further south.

Regional Hydrography

Arctic/Subartic Region: Denmark Strait

Although the main work in the Denmark Strait focused on the deployment and recovery of the moorings listed in Table 4.4, a complete hydrographic section across the Strait was recorded. Fig. 4.8 shows a section of salinity, temperature and density. It depicts the water mass characteristics of the typical current regime in the Strait with an almost vertical separation between the warm, saline water of the Irminger Current to the south-east and the colder water masses from the Greenland Sea to the north-western part of the Strait. The depth-range between 50 m and 150 m defines the East Greenland current, marked by an intermediate minimum in temperature and salinity compared to the centre of the Strait. Below 360 m there is a strong signal of the Denmark Strait Overflow water (DSOW), with higher salinity and temperatures below 0°C. The abrupt decline of the outflow bottom signal at the western end of the section can probably be an artefact of the increasing station-spacing and the resulting uncertainty in the

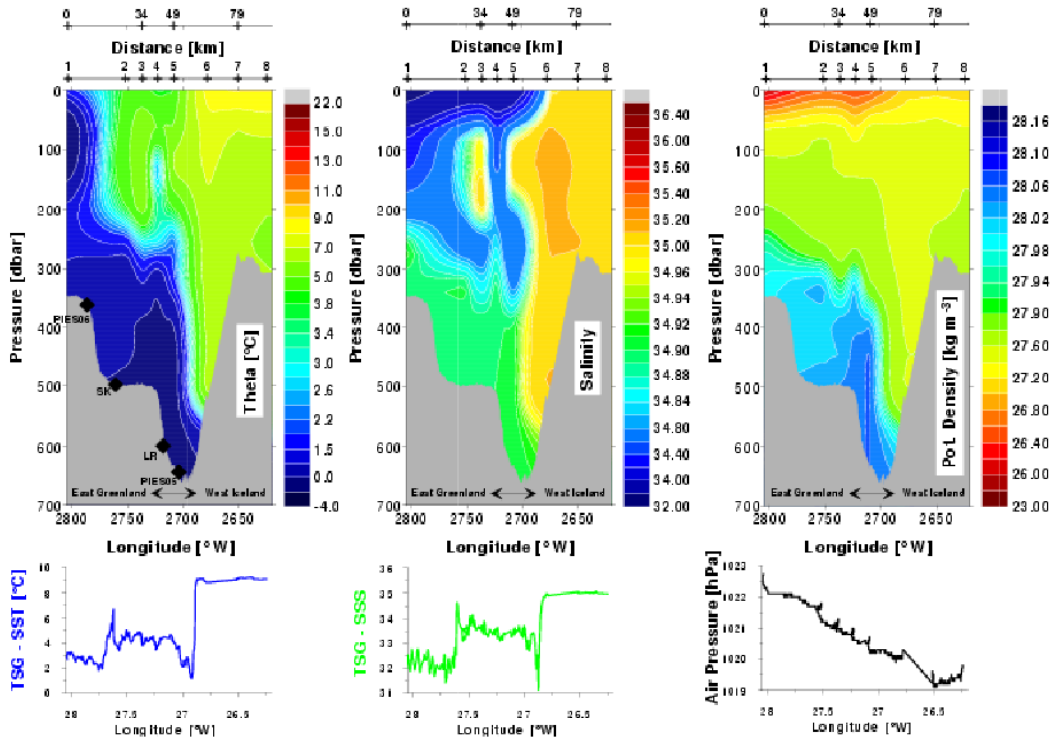

Fig. 4.8: Distribution of potential temperature, salinity and density across the Denmark Strait. In the left picture the longitudinal positions of the moorings deployed in the Strait are marked on the bottom topography, indicating that the outflow of DSOW may be well represented by the moored current meters.

interpolation. In the centre of the Strait the section runs through an eddy structure, which has a thickness of 125 m. This structure should also be visible in the measurements of the vessel mounted **A**coustic **D**oppler **C**urrent **P**rofile (ADCP) covering a depth range from 50 m to 700 m.

Subpolar Region: Iceland Basin

The main scope of the observations in the Iceland Basin was the identification of the pathway of Iceland-Scotland overflow water (ISOW). This water mass spreads along the south-eastern slope of the Reykjanes Ridge. We carried out three sections normal to the proposed pathway of the outflow. The sections are labeled from north to south as **I**, **A** and **B**. Specifically, section **I** covers a mooring line, which carries several recording devices at depth near to the bottom. The station-spacing varied from 30 km to 70 km, with a reduced spacing near the centre of the sections. In all three sections ISOW can clearly be identified by a relatively thin bottom layer, with several local minima, mainly in the potential temperature distribution (Fig.4.9).

The thickness of the bottom layer derived from the conservative tracer data varies between 150 m and 400 m, where the salinity shows a thickness of 150 m. In addition, the salinity distribution exhibits a clear separation of the outflow from the deep background field of the Iceland Basin, characterized by a lower salinity (Fig.4.10). The slope of the 27.99 neutral density surface marks the overflow by a lateral distribution in downward direction. This is also reflected in the disappearence of the 28.07 neutral density surface in the depth-range of 1500 m to 2500 m. Both, the disappearance of the high core densities and the corresponding broadening of the outflow, indicate the presence of active entrainment, enhanced over steep topography, whereas at greater depth the outflow remains a persistent signal on all three sections.

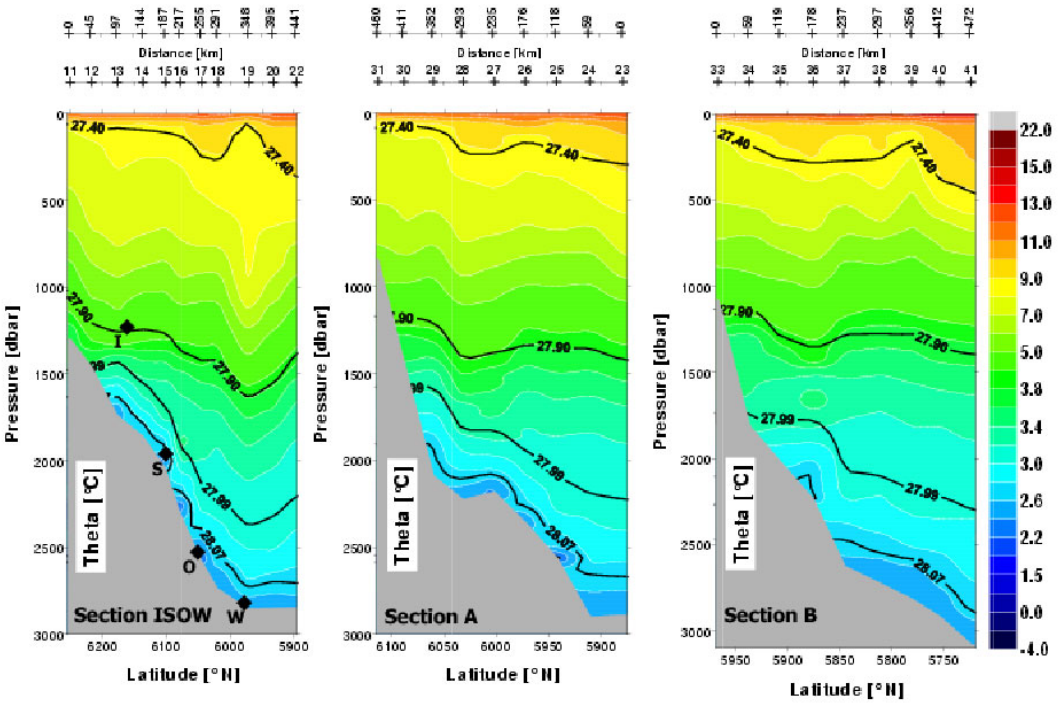

Fig. 4.9: Potential temperature sections in the Iceland Basin. In the left picture the locations of the moorings labeled as I, S, O, and W, are marked at the bottom. These four moorings were launched in spring 2001 and shall be recovered in summer 2002.

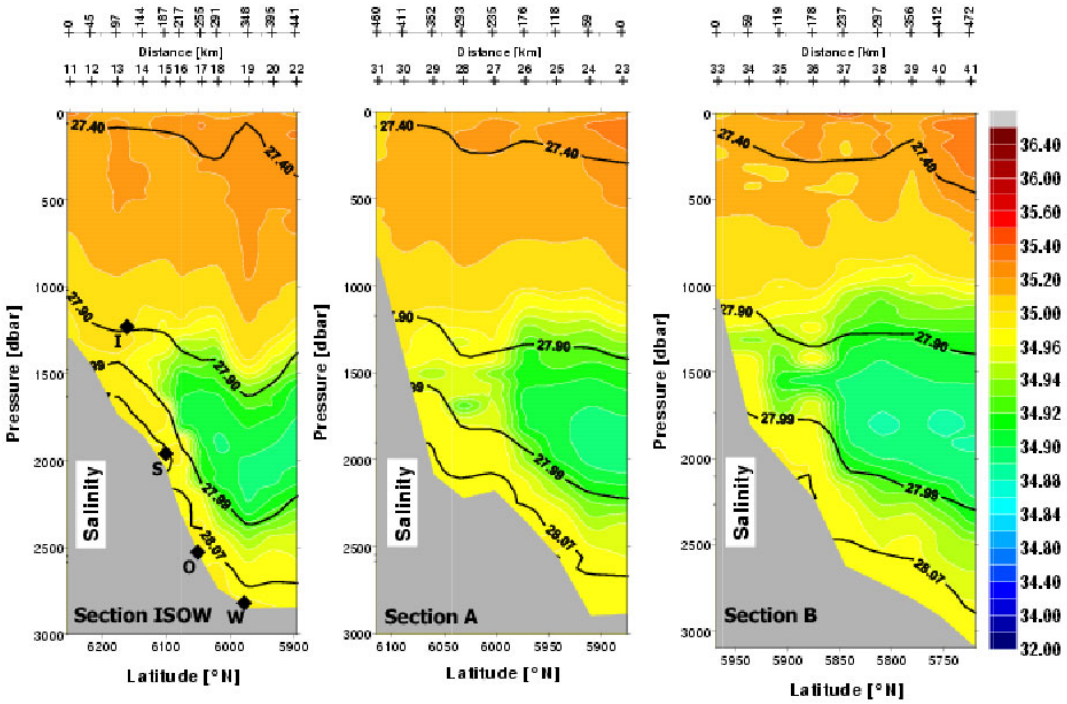

Fig. 4.10: Salinity sections I, A and B in the Iceland Basin.

The comparison of the tracer data of the three sections and the instantaneous velocity data, measured by a lowered ADCP (150 kHz), exhibits for the bottom layer a good agreement between the flow distribution and current direction (Fig.4.11). In general, the velocity data show a more barotropic, i.e. banded structure with local *maxima* at the bottom along the steep part of the topography. These are in good correspondence with the local *minima* in temperature. The maximum current velocity is around 30 cm/s and is directed south-westward. The velocity data were not detided, which accounts for an uncertainty in this region of up to 8 cm/s.

Section **I** runs through an intense eddy structure, with core velocities of up to 40 cm/s. The centre of the eddy is at 750 m. A corresponding local minimum appears in the oxygen data, indicating water masses inside the eddy from a different oceanic region. Fig. 4.12 shows the quasi-synoptic flow field at the bottom of the Iceland Basin. The vectors represent the mean of the lower 100 m of the LADCP profiles. The observed flow field is in good agreement with the current view of the spreading of the outflow along the Reykjanes Ridge. At section I there are high velocities in a relatively narrow region. Lower velocities were observed over a broader region further downstream of the outflow. The alignment of the vectors suggest a local recirculation at the south-eastern end of section **I**. However, as mentioned above, there is an intense eddy perturbation with different water masses at lower levels. This suggests an enhanced recirculation in the bottom layers by a barotropic signal of the eddy. It should be noted that the measurements of the downward looking LADCP do not cover the entire water column. The reflection of the acoustic pulses from the bottom prohibit the sampling in a column 50 m above the bottom. If an increasing velocity signal towards the bottom is detected, it can be assumed that the velocity underestimates the absolute velocity maximum of the bottom trapped outflow current.

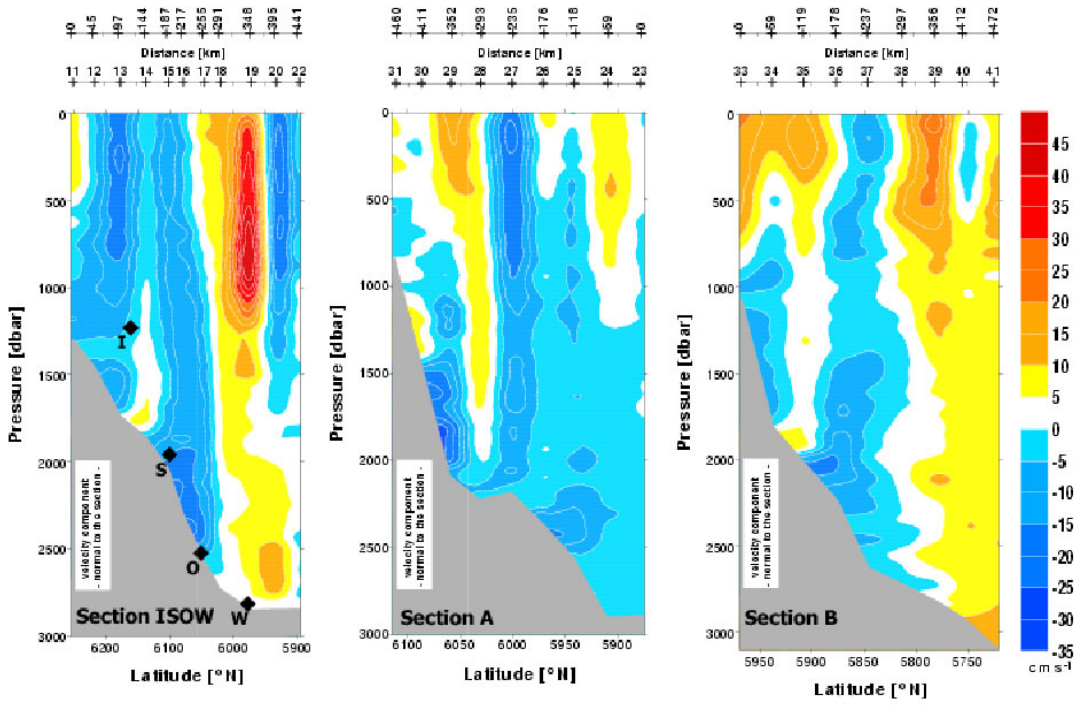

Fig 4.11: Horizontal velocity normal to the sections I, A and B measured by a lowered ADCP (data without compensation of a tidal signal).

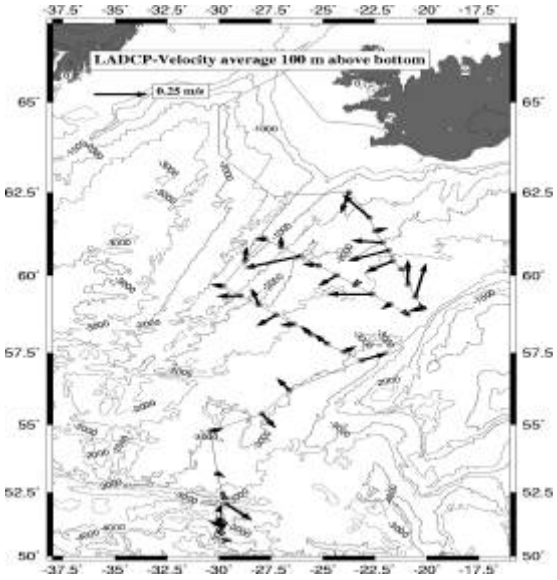

Fig 4.12: Horizontal map of the LADCP-bottom velocities in the Iceland Basin. The vectors define the mean velocity of the hundred metres above the bottom for each profile.

Subtropical Outskirts: Western European Basin

The fourth leg closed with the completion of the eastern part of the WOCE-section A2. This quasi-zonal section covers the North Atlantic from the Newfoundland Banks to the exit of the English Channel. The mean latitude of this section is 45°N. The western part of this section was occupied during leg 1 of this cruise. These two parts together represent the tenth realisation of the section A2 of the World Ocean Circulation Experiment (Fig.4.13 – 4.15). The eastern part of the WOCE/A2-section started at the western slope of the Mid-Atlantic Ridge (MAR). The station-spacing is reduced over both slopes of the Mid-Atlantic Ridge as well as in the eastern boundary current regime. The following water masses are defined by intervals of neutral density surfaces (cf. Lorbacher, 2000).

- SPMW Subpolar Mode Water
- MW Mediterranean Water
- LSW Labrador Sea Water
- ISOW Iceland Scotland Overflow Water
- NADW North Atlantic Deep Water
- AABW Antarctic Bottom Water

The SPMW shows both a negative zonal temperature and salinity gradient. The low-saline and high-oxygen tongue of LSW entering the Iceland Basin through the Charlie-Gibbs Fracture Zone (CGFZ) is best developed around 18°W at a depth of 2000 m. It is absent at the western slope of the MAR. The MW appears at two different depths. The salinity maximum is found at a depth of 1000 m. The lower, though less pronounced of high-saline water, spreads from the eastern boundary into the Iceland Basin within a depths range from 2500 m to 3000 m. This is the expected deep diffusive signal of MW at this latitude. We also found an additional unexpected strong signal of high salinity and higher temperatures directly along the European continental shelf at depths between 700 m and 900 m. The influence of possibly recirculated ISOW can be noticed at the eastern slope of the MAR by an increase in temperature, salinity and oxygen at a depth between 3000 m down to 3800 m.

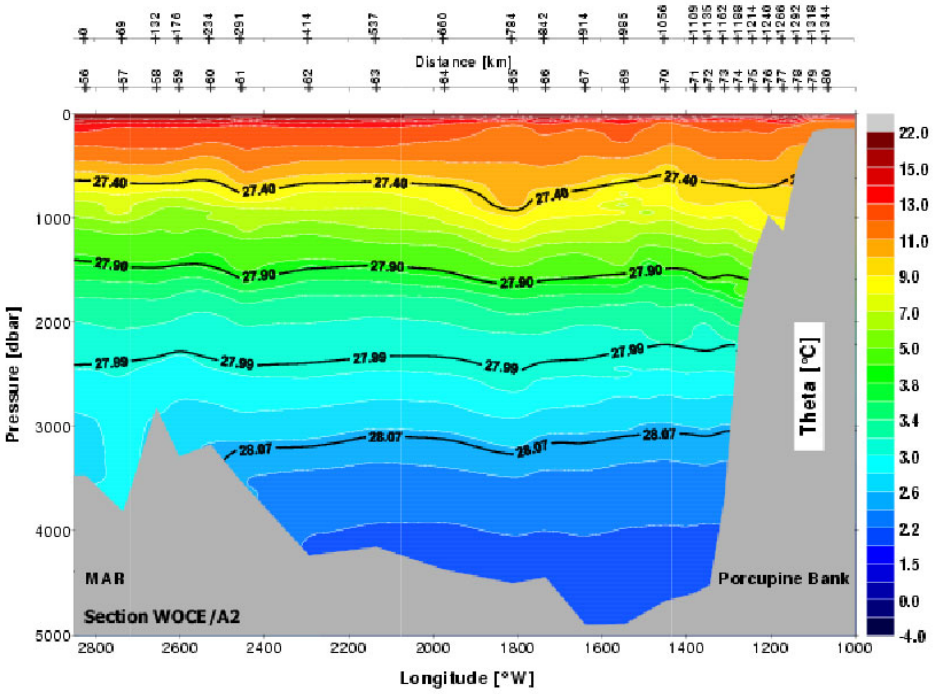

Fig. 4.13: Potential temperature of the eastern part of the WOCE-section A2.

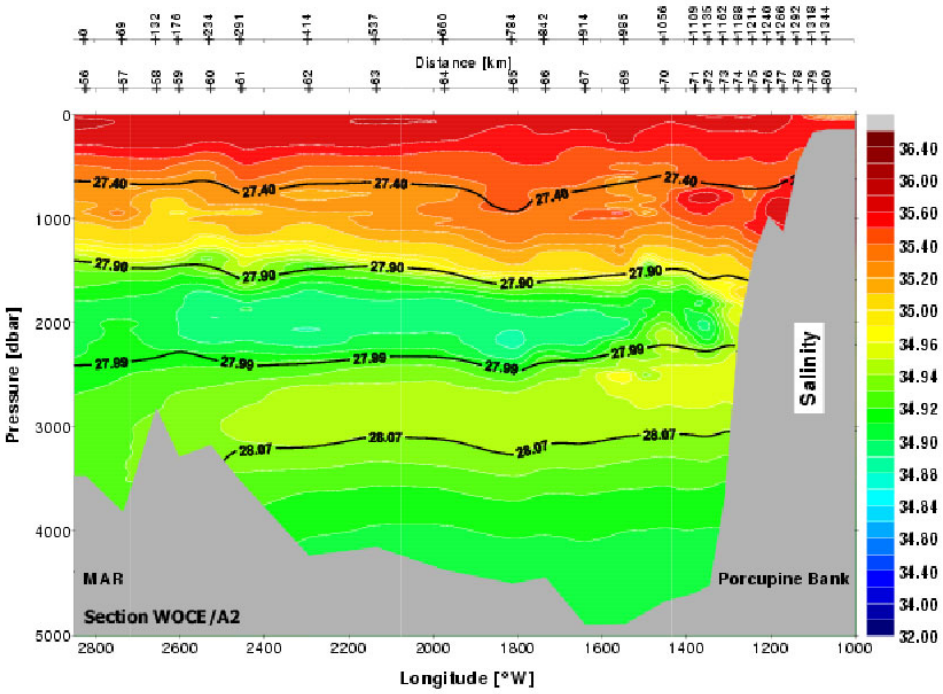

Fig. 4.14: Salinity of the eastern part of the WOCE-section A2.

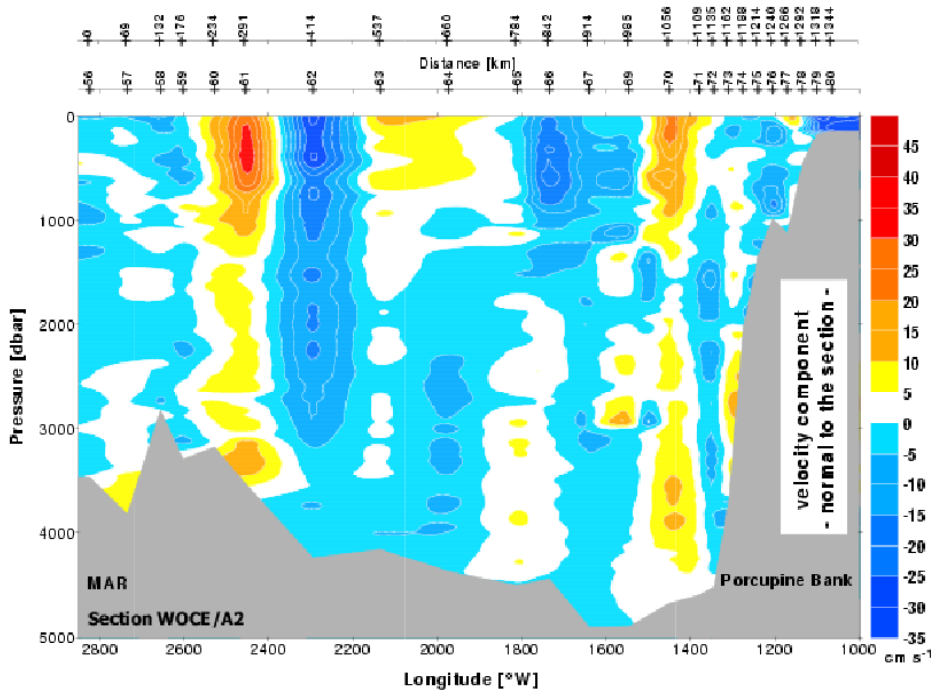

Fig. 4.15: Distribution of meridional velocity from the LADCP measurements for the eastern part of WOCE-section A2.

The instantaneous meridional velocity distribution observed with the LADCP across A2 (Fig. 4.15) shows various eddy structures in the upper water column. The velocities in the centre of the basin are negligible. There are velocity signals directly at the topography corresponding to the northward spreading deep MW at 3000 m at the eastern end of the section. Unexpectedly we also found a northward current at the depth range of ISOW on the eastern side of the MAR, which is in contradiction to the assumed southward spreading of the ISOW along the topography. Nevertheless, it should be noted that the velocities in general are rather low and, as already noted above, the velocity data do not incorporate a tidal correction. The latter may even lead to a reversal of the current direction is this area.

4.4.2 Tracer Oceanography

(M. Bleischwitz, K. Bulsiewicz, R. Steinfeldt)

Material and Methods

During legs 3 and 4 water samples have been collected from 10 liter-NISKIN bottles for the analysis of the **c**hloro**f**luoro**c**arbons (CFC-11 and CFC-12). Additionally on leg 4 Helium samples have been collected into copper tubes. These samples will be measured later with a specially designed noble gas mass spectrometer at the laboratory in Bremen. Measurements of the CFC-concentrations in the water samples have been performed on board using a gas chromatographic system with capillary column and Electron Capture Detector (ECD).

CFC sampling has been performed on 132 stations, and helium samples where taken on 9 stations (Fig. 4.16). A total of 2048 CFC data and 96 helium data have been obtained.

A detector drift affected the accuracy and precison for the CFC-11 data. The blank for CFC-11 and CFC-12 was negligable. Accuracy was checked by analysing 75 water samples at least twice. It was found to be 0.3% for CFC-12 and 0.6% for CFC-11. CFC-contamination of the Niskin bottles was checked at a test station in the deep eastern basin, where all bottles were tripped at the same depth. This water is 'old', exhibiting low CFC-concentrations. All measurements on this station show nearly the same data, which indicates clean Niskin bottles. The CFC concentration of the gas standard used to calibrate the water samples are not reported on the SIO93 scale. This standard gas will be recalibrated at the laboratory in Bremen.

The anthropogenic compounds CFC-11 and CFC-12 have been released into the environment since several decades. The atmospheric release of CFC-11 and CFC-12 started in the 1930s and showed initially exponential increase, since the 1980s the increase is slowing down. Because of their transient nature the CFCs provide time information on the ventilation of water masses.

Helium samples were taken near the Mid-Atlantic Ridge, were sources of methan had been detected. The data will show in how far ^{3}He is also released by these sources and if a correlation between anomalies of methane and ^{3}He exists.

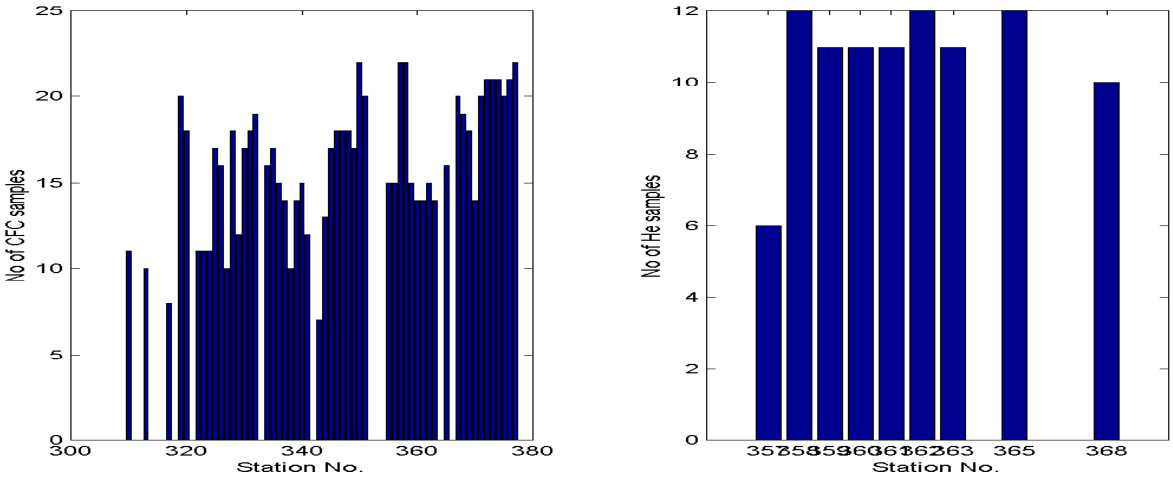

Fig 4.16: Number of tracer samples taken during M 50/4.

Preliminary Results

The tracer investigation along the East Greenland continental slope south of Denmark Strait dur ing leg 3 continues earlier investigations in 1997 and 1999. The main purpose of the sampling was to study the circulation and to analyze the variability of the composition of the Denmark Strait Overflow Water (DSOW).

Figure 4.17 shows the concentration of CFC-12 on the three sections throughout the Iceland Basin **(I**, **A** and **B** from north to south). Both deep water masses (ISOW and LSW) can be found on all three sections. The ISOW is confined to a terrain following boundary layer and shows maxima of CFC-concentration and salinity. It does not reach the deepest part of the Iceland Basin, but spreads along the Reykjanes Ridge. At the southernmost section B the CFC-

concentrations near the bottom are considerable lower (0.1 - 0.2 pmol/kg), supporting the finding that a great part of ISOW leaves the Iceland Basin through gaps in the Reykjanes Ridge into the Western Atlantic. The LSW (density range $27.74<\sigma_0<27.8$ kg/m³ indicated by isopycnals) is characterized by a salinity minimum (dashed line). Whereas temperature and salinity show a linear transition between the ISOW and the LSW, the CFC-data show that these two newly ventilated water masses are separated by older deep water.

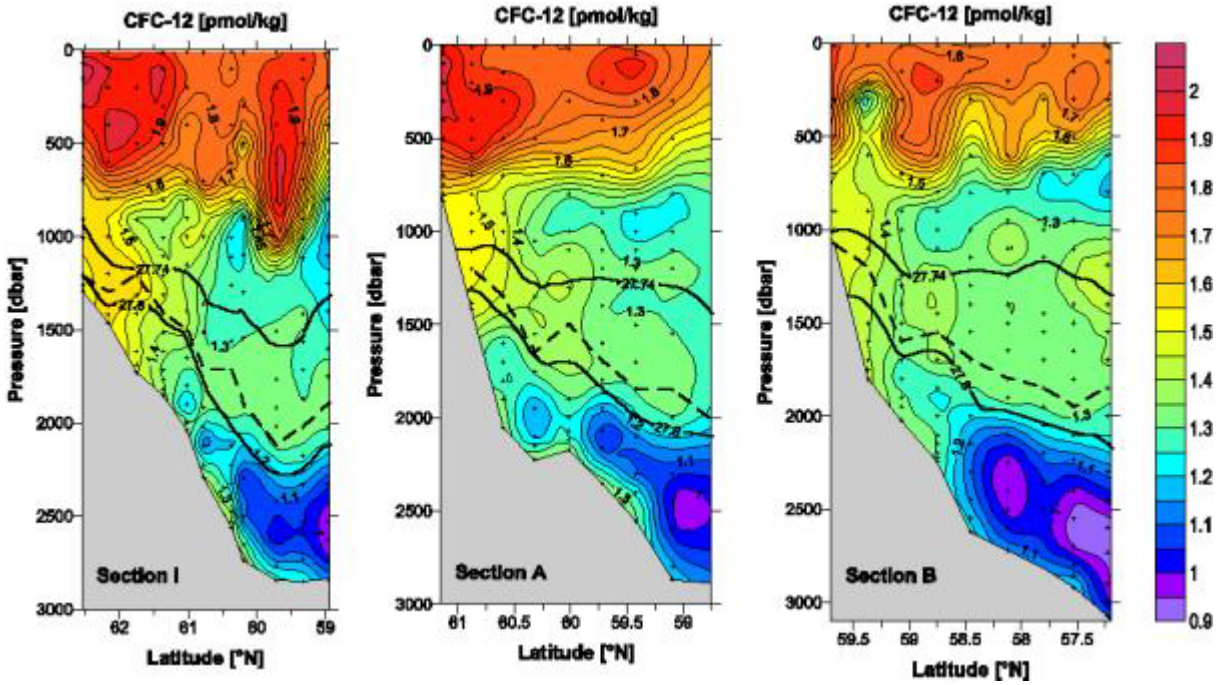

Fig. 4.17: CFC-12 distribution on sections I, A and B in the Iceland Basin.

LSW enters the Eastern Atlantic near the Charlie Gibbs Fracture Zone (CGFZ) and spreads in eastern and northern direction. The northern path can be traced from the comparison of CGFC-concentrations in the LSW-layer at the stations located near the GFZ and on the three sections inside the Iceland Basin (Figure 4.18). The concentrations are highest at the GFZ and decrease weakly from section **B** to sections **A** and **I**, indicating a short spreading time of LSW from the GFZ to the north of the Iceland Basin of only a few years. Not only the CFC-concentration inside the LSW, but also its volume decreases towards the north. Whereas at section **B** a marked core of LSW is present, at sections **A** and **I** a greater amount of more saline water influenced by ISOW can be found in the density range between $27.74<\sigma_0<27.8$ kg/m³.

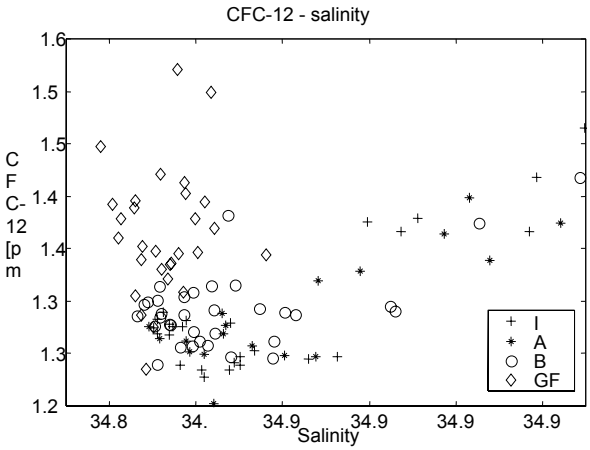

Fig. 4.18: CFC-12 vs salinity correlation in the LSW- density range 27.74<σ_θ <27.8 kg/m³ for different sets of stations. I, A and B: M50/4-sections in the Iceland Basin; GF: M50/4-stations near the Charlie Gibbs Fracture Zone.

4.4.3 Marine Chemistry

(K. Friis, J.D. Afghan, H. Lueger, F. Malien, T. Steinhoff)

On leg 4 the CO_2 group from Kiel (SFB 460, subprogram A5) continued the research program that started on leg 1 and is described above. The same analytical equipment was used and methodologies were applied.

C_T, A_T and pH Quality Control

The quality control of the various parameters of the carbonate system were performed by help of certified reference materials (CRM) and duplicate analysis that were taken approximately every tenth to twentieth sample. These standards are used to determine the accuracy and performance of the systems. The duplicates show the precision of the analytical instrument. For the pH quality control the CRM measurements allows assessment of the long term precision during the cruise as far, as a specific CRM batch is used for the whole cruise. An overview of the quality controls is shown in Tab. 4.1 and in Fig. 4.19 A-F. All controls show a very good agreement with the achievable accuracy and precision estimates according to Millero et al. (1993) (see also leg 1).

Tab. 4.1: M50/4 key data of the discrete C_T, A_T, pH analyses. The CRM measurements give an accuracy estimate, the duplicate measurements a precision estimate.

	C_T	A_T	pH_T $^{21\,°C}$
CRM: Analyzed bottles	50	80	37
Batches used	(52, 48, 36, 35)	(52, 35)	(52)
Mean deviation from certified CRM value	- 0.37 µmol/kg	0.34 µmol/kg	not certified for pH - 0.0023 compared to M50/1
(standard deviation)	(± 1.14 µmol/kg)	(± 2.41 µmol/kg)	(± 0.0023)
Duplicates: Analyzed pairs	81	82	83
Mean deviation from duplicate value	1.1 µmol/kg	2.9 µmol/kg	0.0009
(standard deviation)	(± 1.0 µmol/kg)	(± 2.6 µmol/kg)	(± 0.0009)

Fig. 4.19 shows the analytical C_T and A_T performance during leg 4. A mean deviation of the CRM measurements from the certified value is - 0.37 µmol/kg (C_T) and + 0.34 µmol/kg (A_T). The extreme outliers (station 345 and 351) in the A_T range chart (Fig. 4.19 C) are probably due to smaller instabilities of the emf at the reference electrode. Although the (A_T-) CRM measurements show no obvious deviations from the mean, the A_T profiles of both stations are not that smooth as can be expected from the C_T and pH_T measurements.

The quality control of the spectrophotometric pH determination shows a precision of about ± 0.001 pH units (Fig. 4.19 E and F and Tab. 4.1) and a slightly higher long term precision based on the CRM measurements of batch 52. The mean CRM pH is 0.0023 units lower than the mean pH on leg 1, but it is although comparable to the CRM pH in the end of leg 1. This holds on the speculation of an aged platinum resistance temperature probe, that has been mentioned above and will be controlled later. Nevertheless an uncertainty of ± 0.002 pH units corresponds with a C_T and A_T uncertainty of about ± 1 µmol/kg and seems to be acceptable with respect these parameters.

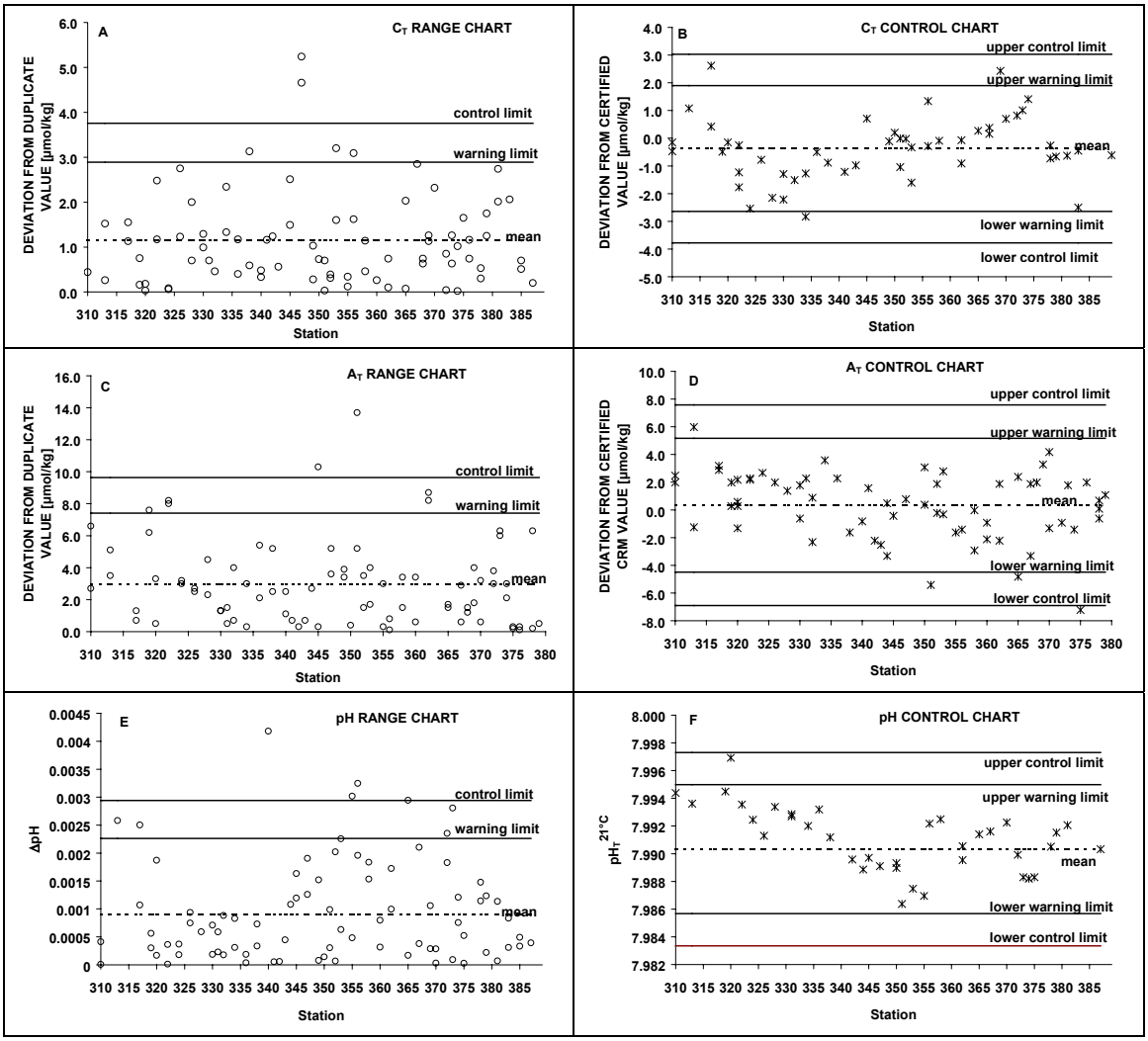

Fig. 4.19: A-F: Quality charts for C_T, A_T and pH_T analysis The range charts on the left-hand side are based on duplicate analysis of usually two niskin bottles per hydrocast. The control chart on the right-hand side are based on measurements of certified reference materials (CRM), that was at minimum one control measurement per hydrocast and parameter. Also shown are ‚warning' and ‚control limits', these are included according to a standard procedure for marine CO_2 parameter analysis in DOE (1994). The ‚warning limits' result in muliplying the standard deviation by two and the ‚control limits' by three. About 95 % of the plotted points should be within the warning limits.

Preliminary results of the C_T, A_T and pH analysis

A total number of 832 (n = 745) C_T samples, 798 (n = 723) A_T samples, and 850 (n = 768) pH samples we analyzed. A list of all stations where samples have been taken can be found in the listings.

For meridional transport calculations the transatlantic WOCE-A2 section has become a key section for the North Atlantic. The sections position is in between the subtropical and subpolar gyre at about 45 °N and describes the hydrographic situation of the meridional overturning cell near to regions of water mass formation. An overview of the A_T and C_T measurements on the quasi-zonal section is shown in Fig. 4.20. The **a**pparent **o**xygen **u**tilization [AOU = O_2^{sat} –

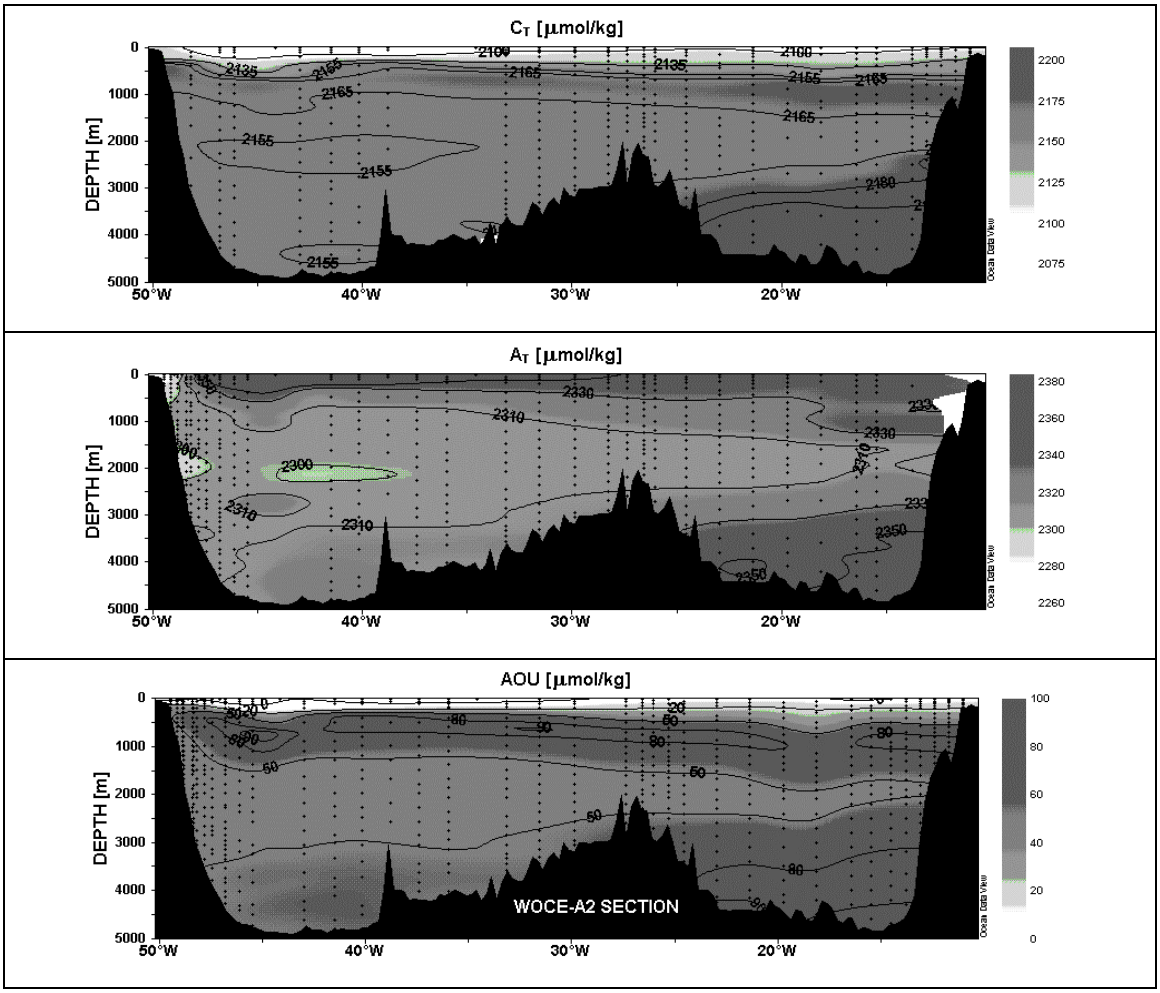

Fig. 4.20: Distribution of A_T and C_T and apparent oxygen utilization (AOU) on the transatlantic WOCE-A2 section. A back-calculation technique based on these parameters leads to an estimate of the ‚full' anthropogenic CO_2 signal, i.e. the additional CO_2 uptake from the beginning of the industrial revolution up to now (Poisson and Chen, 1987).

O_2^{meas}] in the third plot, is a direct measure of the respiration that took place in a water mass. High respiration (AOU) terms correspond with highest C_T and A_T values in the bottom waters of the eastern basin and indicate the old Antarctic Bottom Water component. Lowest AOU values at the sea surface agree with low C_T values and show the influence of photosynthesis on the carbonate system. CO_2 is transformed to organic carbon and therefore can not be seen by the inorganic C_T parameter. High A_T values in the sea surface express the minor influence of photosynthesis on this parameter. The surface near A_T values are mostly dependent on salinity (Friis, 2001) and in a minor part on temperature and biological processes of calcification and CO_2 assimilation/respiration. Below ~1000 m salinity changes are small with respect to carbonate chemistry and increasing A_T values with depth got an explanation by aragonite and calcite dissolution, that amplifies with depth and water mass age. In context of hydrology the three parameters in Fig. 4.20 mainly state the carbonate system. Therefore they are essential for different back-calculation techniques for the determination of anthropogenic CO_2 (Chen and Millero, 1979; Poisson and Chen, 1987; Gruber et al., 1996).

Preliminary results of the fCO_2 measurement

On leg 4 approximately 13.000 data points of sea surface (~5 m) pCO_2 and about 800 data-points of atmospheric pCO_2 were collected. Additionally ambient air pressure, sea surface temperature and sea surface salinity were measured. The results were already corrected on basis of three standards and transformed into the fugacity of CO_2 (fCO_2) in order to account for the non-ideal behavior of carbon dioxide as a gas. The fCO_2 of seawater is a function of temperature, total inorganic CO_2, alkalinity and salinity.

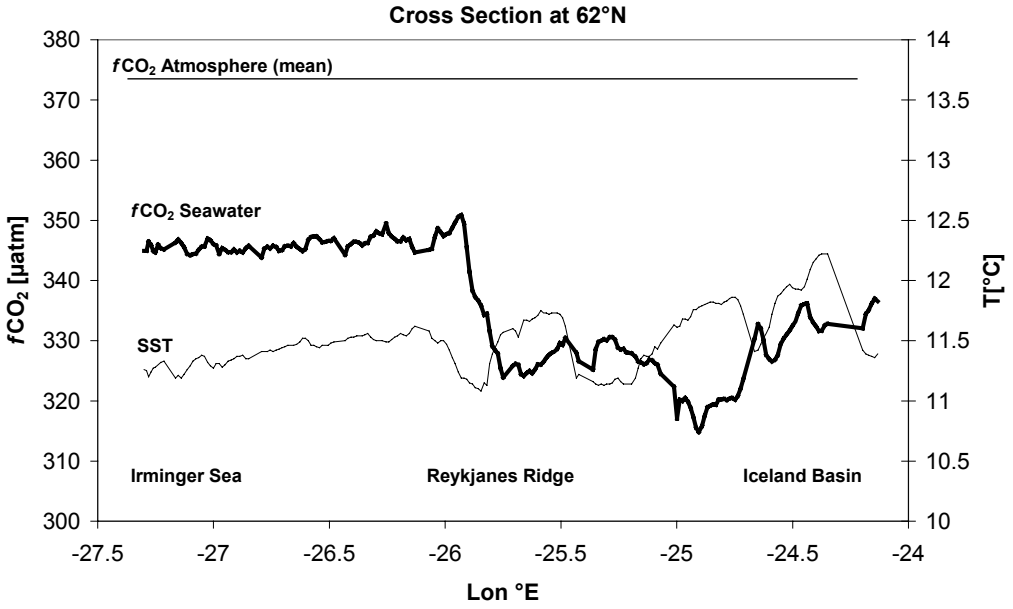

Fig. 4.21: Results of the continuous measurement crossing the Reykjanes Ridge at 62°N. The atmospheric fCO_2 data were averaged.

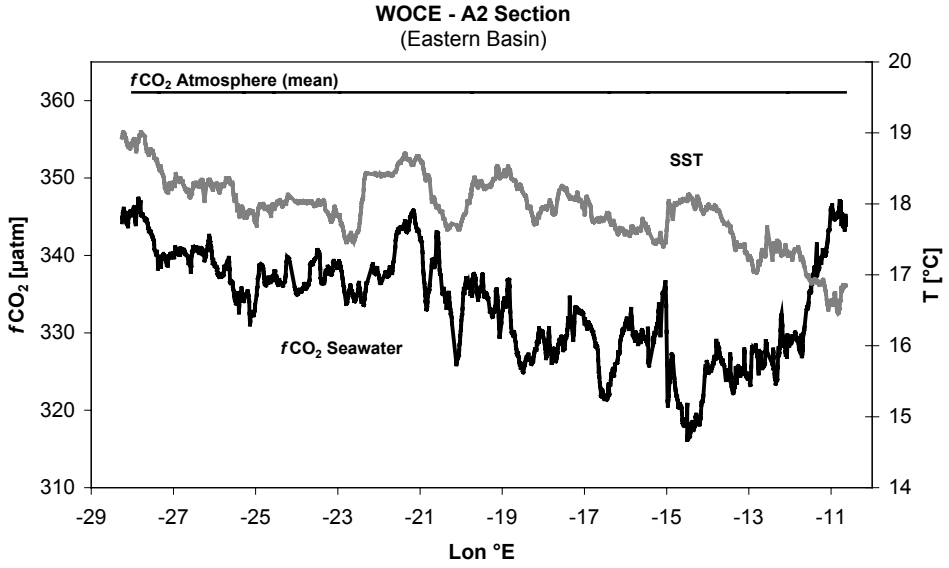

Fig. 4.22: Results of the fCO_2 measurement along 48°N. The first part of this section was measured during M50-1. The atmospheric fCO_2 data were averaged.

In open-ocean surface waters with only small changes in the alkalinity and salinity, the fCO_2 is primarily governed by changes in temperature and total inorganic CO_2 concentration (Stephens et al., 1995). The effect of temperature on the fCO_2 has been directly determined: the fCO_2 of seawater doubles for every 16°C increase in water temperature (Takahashi et al., 1993). In the North Atlantic one also finds that the fCO_2 varies over short distances. These variations can be attributed to patchiness in biological activity and episodic mixing events. The latter are correlated with chlorophyll concentrations and sea surface temperature, respectively.

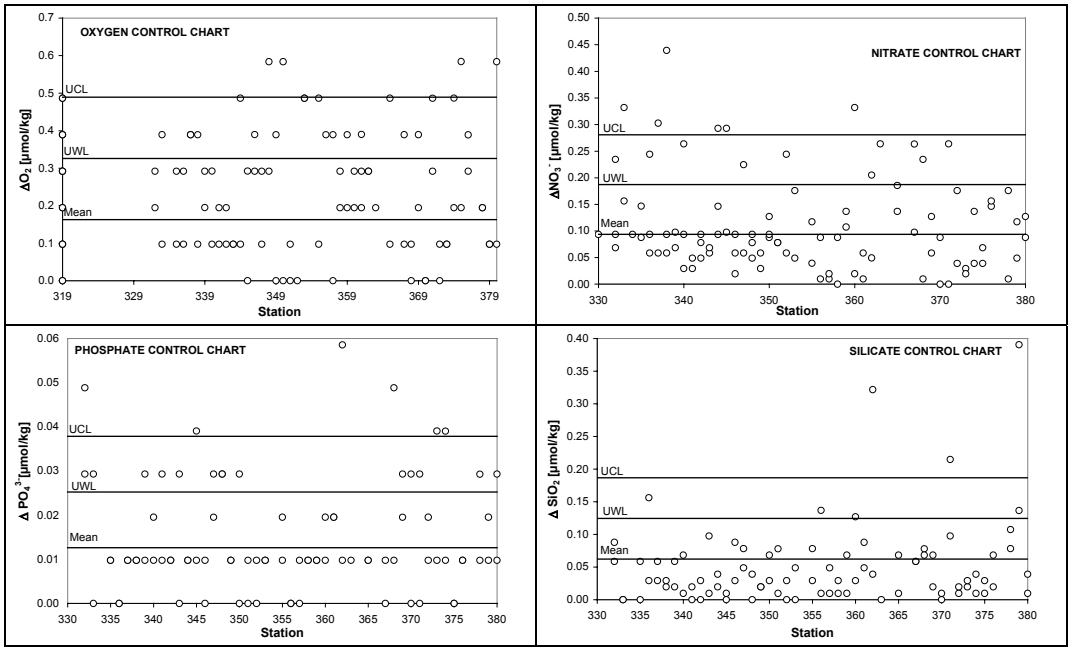

Fig. 4.23: Control charts for nutrients and oxygen (with mean deviations and control limits, see Fig. 4.20). The charts are based on measurements on duplicate samples.

The M50/4 cruise led us to the northern parts of the Irminger Sea, Iceland Basin and the eastern part of the WOCE-A2 section.

The section from the Irminger Sea to the Iceland Basin with a crossing of the Reykjanes Ridge is shown in Fig. 4.21. There is an obvious separation of the surface regimes of the two basins and the fCO_2 decreased by about 20 µatm in the Iceland Basin. The fCO_2 variability (differences of up to 50 µatm) is quite high and most of the time not thermo-dynamically related to the sea surface temperature.

The last part of the cruise went along the WOCE-A2 section. The corresponding fCO_2 results are shown in Fig. 4.22. Along this track there is a more or less constant undersaturation of about 30 µatm for the seawater fCO_2 compared to the atmosphere. The seawater fCO_2 follows most of the time the thermodynamic direction of sea surface temperature. The CO_2 fugacity reaches values as low as 316 µatm. Where a fCO_2 decrease does not have a counterpart in the sea surface temperature line probably biological activity is reflected. During a plankton bloom CO_2 fixation takes place and seawater fCO_2 values usually decrease to lower than 300 µatm. Hence Fig. 4.22 could record the beginning or the end a plankton bloom where the photosynthesis rate is reduced. The strong fCO_2 increase at about 14 °W to the European shelf can be explained by a inorganic (i.e. remineralized organic) freight along the continental margins.

Sample Collection and Storage of ^{13}C, ^{14}C, TOC and Chlorophyll Samples
On leg M50/4, 395 samples for ^{13}C mass spectrometer analysis were collected. Based on the ^{13}C data a priority list will be made for about 75 samples for ^{14}C mass spectrometer analysis, that can be done from the ^{13}C sample extract. Furthermore 194 TOC samples and 112 chlorophyll samples were stored.

Nutrients and Oxygen
Nutrients (nitrate, nitrite, phosphate, silicate) were determined from 1242 Niskin bottles. The nutrient analysis was made with an autoanalyzing system according to Grashoff et al. (1999). The accuracy for nutrient analysis was approximately 1 % of the nutrient standards. For precision estimates duplicate samples were taken and analyzed at about every tenth sample (Fig. 4.23). The corresponding accuracy and precision (± standard deviation / in brackets) estimates were 0.205 (± 0.09) µmol/kg for nitrate, 0.005 µmol/kg for nitrite, 0.025 (± 0.013) µmol/kg for phosphate and 0.5 (± 0.06) µmol/kg for silicate.

Oxygen was analyzed on 1270 niskin bottles according to a standard titration after Winkler (Grashoff et al., 1999). The measurements were done with a precision of ± 0.16 µmol/kg.

4.4.4 Methane analyses, seafloor observations and bathymetric mapping

(J. Greinert , K. Fürhaupter , B. Bannert)

The major task of the methane measurements during M50/4 was the study of methane plumes in the Mid-Atlantic-Rift Valley south of the Charlie-Gibbs-Fracture Zone (RV-CGFZ). Here, methane concentrations of 5 to 7 ppmv were observed between 2900 and 3200 m water depth during M39 and PO261 at two stations. These concentrations are up to four times enriched compared to the observed concentrations of approx. 1.5 ppmv usually found at this water depth. The higher concentrations were first discovered during METEOR cruise M39 in 1997 at station M39-260. Three years later the same position was sampled during cruise PO261 of FS POSEIDON (station 176), and equally high amounts of methane were found. At station PO261-170 further south, even higher concentrations of up to 7 ppmv were detected, and this raised questions: Where does the methane originate from, what is the source and are the methane expulsions permanent or temporary?

To get more information about the methane distribution, seven CTD casts were performed within the Rift Valley, two of them at the previously sampled stations. It was planned to use a TV-guided camera sled (OFOS) to observe the seafloor after the area with the strongest methane enrichment was found. Surveys with the multi-beam echosounder Hydrosweep were undertaken to map the seafloor where we hoped to find signs of the methane source during the OFOS observations. One possible methane source at mid ocean ridges is the mineral re-crystallisation of olivine to serpentine and magnetite which is called *serpentinisation*. This typical process at ultramafic rock hosted hydrothermal areas generates methane by CO_2 reduction with hydrogen released from the serpentinisation:

$$6[Mg_{0.5}Fe_{0.5}SiO_4] + 7\ H_2O \rightarrow 3[Mg_3Si_2O_5(OH)_4] + Fe_3O_4 + H_2$$

$$CO_2 + 4H_2 \rightarrow CH_4 + 2H_2O$$

In addition, the use of the OFOS system during M50/4 also served as a test for METEOR cruise M52 to the Black Sea during which seafloor observations will be an essential part.

In addition to our observations at the RV-CGFZ, we sampled and analysed CTD stations on all hydrographic sections, which were conducted in order to trace water masses using other chemical parameters as well. All in all we took samples from 50 CTD stations, deployed the OFOS once for a 2-mile long track and recorded multi beam data along approx. 200 miles at the RV-CGFZ.

Methods

Methane analyses

For the gas extraction we took water samples (1.2 l) from the CTD rosette in pre-evacuated 2 l glass bottles. In a degassing line these glass bottles were filled with supersaturated salt water and the escaping gas volume was measured in a burette. Gas samples were taken by gas-syringe and methane was analysed with a GC (*SHIMADZU*). The remaining gas was transferred to evacuated ampules for methane source reconstruction via isotope analyses which will be performed on shore. Before and after water samples from a CTD were measured we analysed at least three samples of a calibration gas which gave a accuracy of the GC analyses better than 0.05 ppmv or 3 %. The accuracy of the whole degassing method strongly depends on the goodness of the vacuum in the glass bottles for water sampling and their tightness. Unfortunately some samples were contaminated by atmospheric methane, which is particularly seen in higher gas volumes (> 24 ml). Those analyses were not used later.

OFOS

The Ocean Floor Observation System (OFOS) is used for TV-guided online observation of the seafloor. OFOS, an aluminium frame of 165 x 125 x 145 cm was equipped with a BW video camera, two Xenon lamps (OKTOPUS), an underwater slide camera with flash (BENTHOS), two laser pointers (OKTOPUS) and a FSI memory CTD. The telemetry works with 500 V and a separate cable for grounding was fixed between the telemetry and the wire and for additional security high voltage was switched on after the OFOS was in the water and was switched off before OFOS came on deck. For the seafloor observations themselves, OFOS is towed by the ship along a predefined track at less than 1 kn, and the distance to the bottom is manipulated by the winch. The observer can take slides manually via the deck unit and the video signal is permanently recorded on videotapes. Unfortunately the quality of the video signal was not as good as it could be. This depends on the electrical noise induced by electrical ship devices into the wire of winch 12. In particular we found a strong noise signal from the thermosalinograph in lab 7. Other possible sources of electrical noise could not be determined.

For further deployments and OFOS campaigns it is strongly recommended to shorten the wire of winch 12 to a maximum length of 8 km. Nevertheless, the deployment of OFOS showed that it and other TV-guided devices can be generally used successfully onboard FS METEOR.

HYDROSWEEP

One prerequisite for OFOS deployments is knowledge of the bathymetry. Thus we mapped the area at the R-GFZ where the OFOS might have been deployed by using the HYDROSWEEP system installed on FS METEOR. The data were roughly post processed using the software package 'HYDROMAP' and plotted with 'GMT'.

Results

Rift Valley south of the Gibbs-Fracture-Zone

The map in Fig. 4.24 shows the position of the CTD stations at the RV-CGFZ. At all stations higher methane concentrations were analysed between 2500 and 3600 m water depth with increasing concentrations to the south. In contrast to the former three stations, the concentrations did not exceed 4 ppmv and six of them did not even exceed 3.4 ppmv (Fig. 4.25). Nevertheless a significant methane signal was present at all stations. As shown by the methane distribution in Fig. 4.26, the rather equal methane signals below 2500 m water depth can be interpreted as methane generated further south, which slowly migrates to the north along the rift axis but below the rift crests, which form a 'methane-protecting' basin. The rift crest is generally above 2500 m water depth but shows a depression on the westward flank near 51.1°N were it drops down to 2700 m. This might be the reason for the depression of the upper 2 ppmv boundary in Fig. 4.26 at station M50-363 and may indicate that the bathymetry is an important factor for the methane distribution in rift valleys. The non-occurrence of higher methane concentrations further shows that methane generation by hydrothermal processes is not a permanent process and changes in time and space.

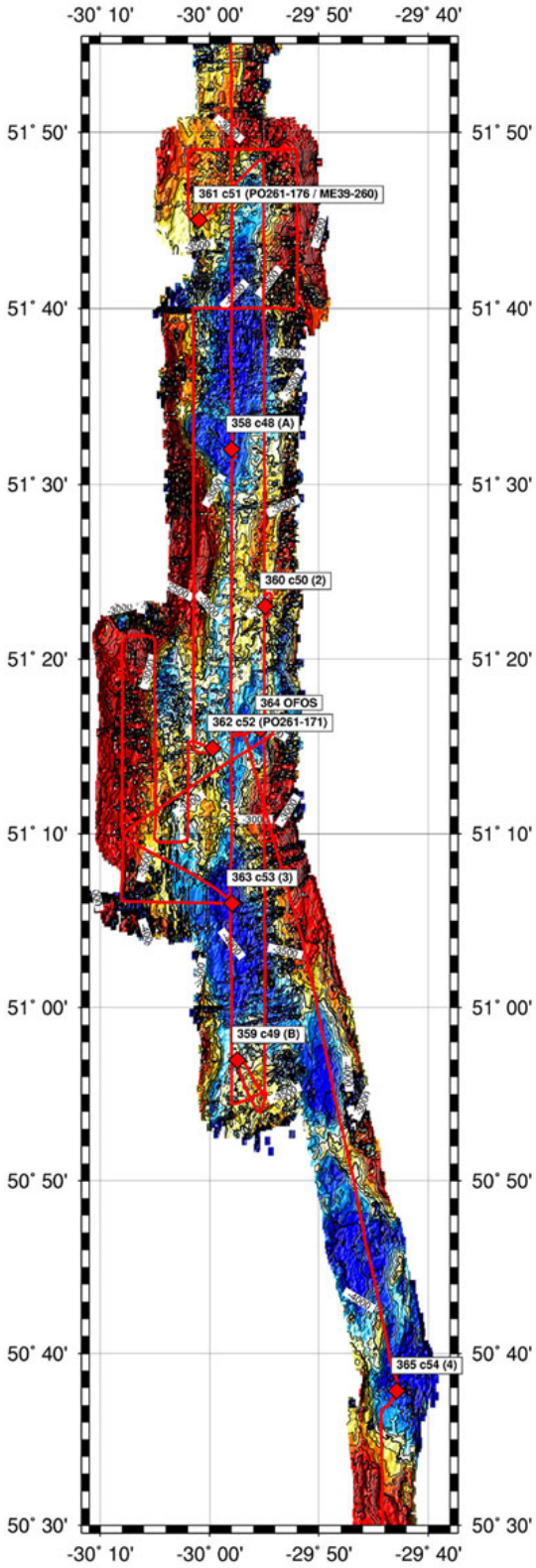

Fig. 4.24: Bathymetric map of the RV-CGFZ area with cruise track (red line) and CTD Stations. The bathymetric data are not yet edited.

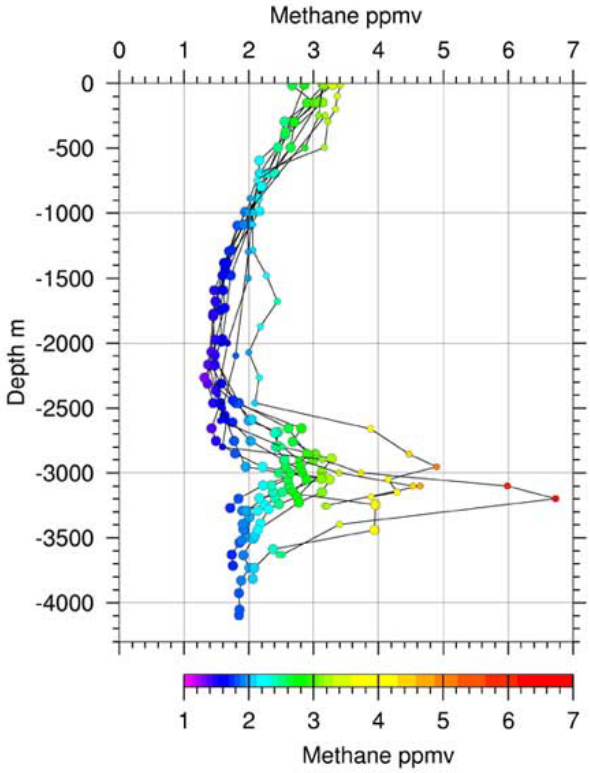

Fig. 4.25: Methane concentrations of all CTD stations at the RV-CGFZ. Smaller circles mark the samples from earlier soundings: PO261 and M39.

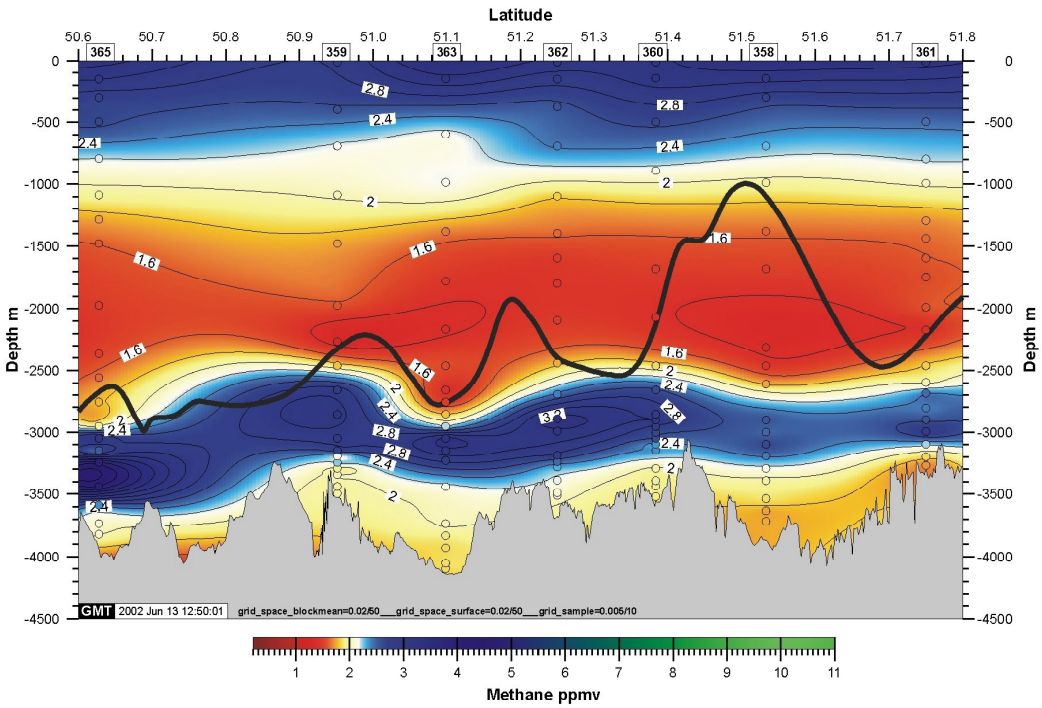

Fig. 4.26: Section of the methane distribution at the RV-CGFZ area, which shows significant methane enrichment below 2500 m water depth. The black line represents the western rift crest (taken from the gravimetric data published by Sandwell and Smith) indicating a relation between the seafloor morphology and the methane distribution.

After sampling CTD station 363 we deployed the OFOS at a rather shallow area at the eastward side of the rift valley, knowing that this area is below 3500 m water depth and thus below the methane maximum. However, we towed the OFOS for 2 miles above the bottom, which showed a small-scaled rough topography with up to 30 m high ridges build up by pillow lava (profile in Fig. 4.27). We found no visible signs of active hydrothermalism, but the OFOS system was successfully tested.

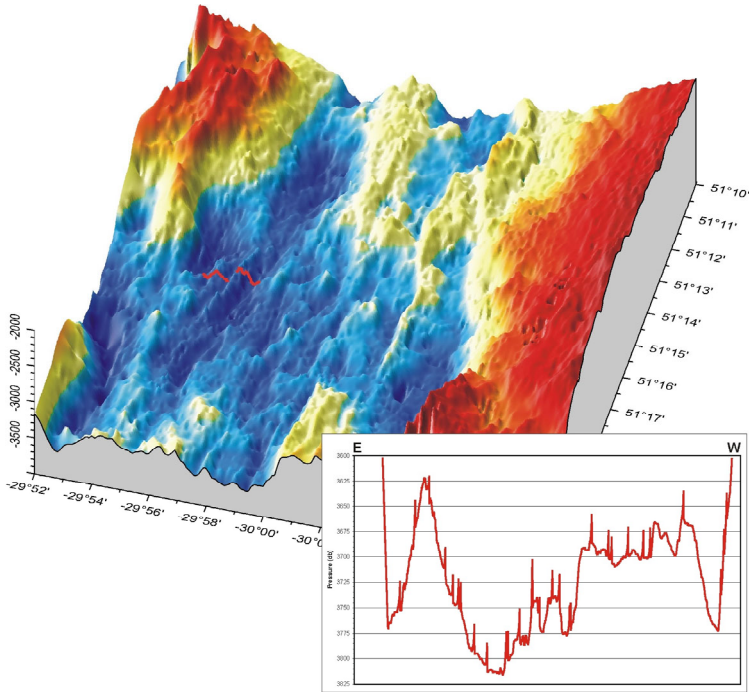

Fig. 4.27: 3D view of the Mid-Atlantic Rift valley (main figure) between 51°10' and 51°21' N showing axis parallel smaller ridges which were crossed by the OFOS deployment. The inserted pressure profile (right corner) was recorded by the FSI memory CTD. Spikes represent rapid heave movements.

Along section **A** in the Island Basin we sampled and analysed data from six CTD stations. The concentrations above 1500 m water depth appear to be typical for this area. The slightly increase below 1700 m at stations 336, 338 and 339 likely represent the ISOW correlating with increased salinity concentrations (Fig. 4.28).

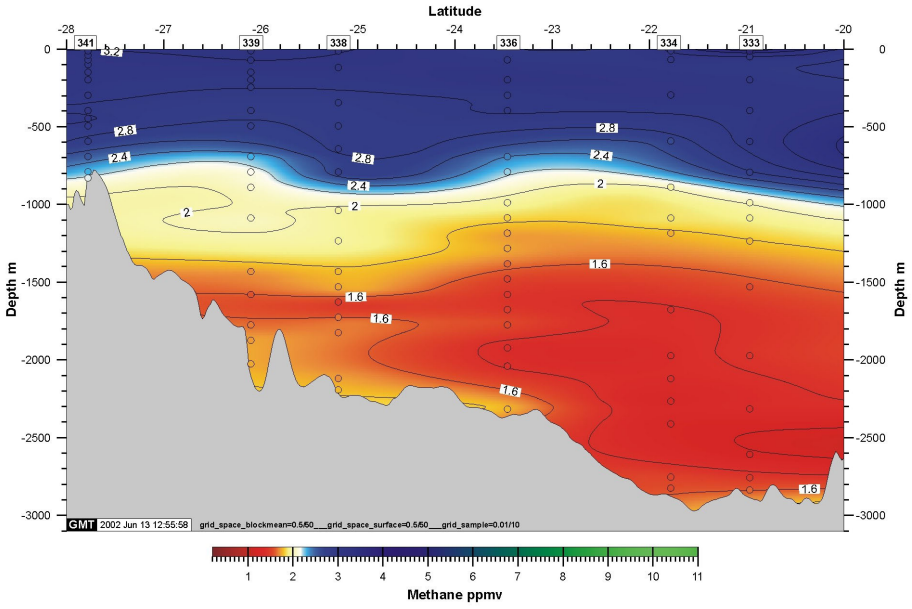

Fig. 4.28: Methane distribution at Section A, Island Basin.

Methane Distribution along WOCE A2

The general methane distribution at the WOCE A2 section shows a continuous decrease from 3 ppmv at the surface and 0.4 ppmv at the abyssal plain. At Station 368 located in the rift valley, we analysed again higher methane concentrations of up to 2.3 ppmv between 2000 and 3100 m water depth below the rift crest. This is similar to the concentrations from the RV-CGFZ area and likely represent a usual phenomena of elevated methane concentrations in rifts of mid ocean ridges. However, the highest methane concentrations during M50/4 were measured at the continental slope between 500 and 1000 m water depth at Station 387 with values of up to 10.14 ppmv. Up to now we do not know the source of these high methane concentrations. The forthcoming stable isotope analyses may provide an indication as to this methane source.

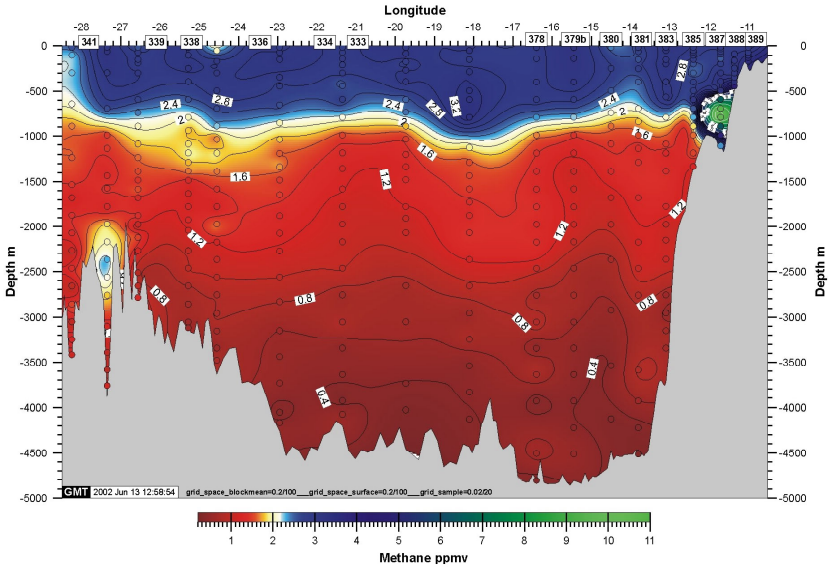

Fig. 4.29: Methane distribution at WOCE A2. Higher methane concentrations were analysed again in the rift valley and at the continental slope with more than 10 ppmv.

4.4.5 Natural Radionuclides

(J. Schaftstall, J. Scholten)

Natural radionuclide are useful tracers for the investigation of the pathways of particle reactive matter in the water column. Their major advantage is their well known production rate in the water-column; and information on particle residence times and scavenging rates can be obtained by comparing the concentration of e. g. ^{230}Th with its production rate from the decay of ^{238}U . In contrast to most of the oceanic environments the North Atlantic is characterised by relatively rapid ventilation of deep water masses which has a severe influence on the distribution of particle reactive elements.

In order to investigate the interannual changes in the concentration as well as the distribution of ^{230}Th along the flow path of the Labrador Sea and Island-Scotland Overflow water masses water samples were obtained during the Meteor cruise 50/4 in the Iceland Basin, near the Charlie-Gibbs Fracture Zone and on a transect along 48° N (cf large circles in Fig. 4.1).

Water samples were sampled in up to seven depth levels between 100m and 3000m. About 10 l of water were filled in pre-cleaned plastic containers, acidified and stored for further analyses in the home labs.

Table 4.2: Locations of radionuclide water samples

Station M50/4	No.	Bottle	Depth (m)	Station M50/4	No.	Bottle	Depth (m)
327	1	21	100	**332**	1	13	100
21°51.0E 60°46.9N	2	19	500	20°11.9E 58°58.9N	2	11	500
2292 m	3	17	700	2827 m	3	9	700
	4	14	1000		4	7	1000
	5	10	1500		5	5	1500
	6	6	2000		6	4	2000
355				**366**			
30°04.9E 53°12.2N	1	17	100	29°42.1E 48°59.7N	1	10	100
3116 m	2	20	500	3025	2	9	500
	3	15	700		3	8	700
	4	13	1000		4	7	1000
	5	10	1500		5	5	1500
	6	7	2000		6	4	2000
	7	3	2800		7	2	2800
370	1	21	100	**379**	1	6	100
26°02.1E 46°60.0N	2	17	500	15°26.9E 48°33.0N	2	5	500
3257	3	14	1000	4790	3	4	1000
	4	10	1500		4	3	1500
	5	7	2000		5	2	2000
	6	3	3000		6	1	3000

4.5 Weather and Ice Conditions during M50/4

When METEOR left Reykjavik heading for Denmark Strait on July 17, there was a gale center of 990 hPa near of Cape Clear, Eire, dominating all of the Western Approaches as well as the Bay of Biscay. A secondary low of 1009 hPa was situated at 58 North 24 West, whereas highs could be found of over 1025 in the Norwegian Sea and the Azores High of 1033 hPa, extending a wedge of 1025 hPa to 56 North 40 West. As the high over Greenland was not very strong, the ship experienced light easterly winds while working in Denmark Strait, these only temporarily being up to 6 Bft on July 19 and thus not hampering operations. The Ice Conditions were such that one of the mooring arrays to be retrieved and employed again could not be reached. An ice promontory rendered the ship's movement in that direction impossible so that the mooring array had to be left unserviced.

The next regions where hydrographic work was being carried out were the Reykjanes Ridge and the Iceland Basin. After retrieval of mooring arrays being deployed by POSEIDON a year earlier two hydrographic sections were made, these being repetitions of sections A and B done during M39 four years ago, thus enabling comparisons of conditions varying with time. The sections ranged from the Rift Valley of the Reykjanes Ridge through the Iceland Basin to its eastern margin. While the METEOR was working, winds were moderate, and direction was varying. The exception was July 26 when a complex gale center of 980 hPa had developed south of Greenland, extending a warm front to our research ship's position so that we observed

southeasterly gales up to 7 Bft, veering to strong southwesterly winds 6 Bft the next day. By then, one gale center had turned northeast into the Irminger Sea where is started to fill. The METEOR experienced lesser winds only on July 27 when a minor secondary low passed her. This was not the only one of its kind, however, for during July 28 another wave along the cold front developed quickly into a gale center of 988 hPa near southeastern Iceland so that at the vessel's position southwesterly gales up to 8 Bft were experienced. By July 29, winds were down to westerly 5 Bft again. The new gale center then dominated the Norwegian Sea for quite a few days.

The METEOR had by now reached her next area of investigation, the 'GEOMAR-Box' in the Charlie Gibbs Fracture Zone (CGFZ). The CGFZ has two abyssal channels connecting basins on both sides of the Mid Atlantic Ridge, and the GEOMAR-Box contains a valley connecting those two channels, thus separating the relative high elevation between the channels into two hills. So the CGFZ and the 'GEOMAR-Box' are key areas regarding exchange of water masses in the deep in a zonal direction. As the METEOR took her time probing this area, winds were light and variable during July 30 due to a wedge of high pressure extending from the Azores High. This prominent feature of the synoptic chart had strengthened to 1033 north of the archipelago so that the next low to migrate east from Labrador had to stay north of the 55th parallel, its intensity of 1010 hPa varying little. For our ship this meant moderate westerly winds during July 31 and August 01.

There was one task still to be done: During M50/1 a hydrographic section had been surveyed extending from about 42 North 46 West to 46 North 30 West. This had been the western part of the WOCE-Project A2 hydrographic section, and now in M50/4 the research vessel completed it across the West European Basin and up the shelf regions south of Eire. It took the METEOR up to August 07 to reach a position just east of where she had turned to Labrador during M50/1 and to complete that section. During these Days the Azores High concentrated on the Archipelago again and weakened somewhat. Meanwhile a low had formed on the U.S. Eastern Seaboard and moved northeast, its central pressure being down to 1015 hPa south of Newfoundland on August 02. Another Low moving east from the area west of the Hudson Bay had intensified to 995 hPa over Labrador. This one intensified further to 990 on August 03, and it managed to integrate the low from Newfoundland into its circulation. In this way it gained an influx of subtropical air masses, and therefore it intensified to 985 hPa on August 04 southwest of Greenland. Our ship experienced moderate westerly winds, backing during that day. The gale center stalled and began filling, and only when central pressure had reached 995 hPa again it continued to move east on August 05. The low slowly filled further, METEOR observing moderate to strong southwesterly winds until the low reached Eire on August 07, central pressure being 1000 hPa. By then its cold front had passed our ship so that strong westerly to northwesterly wind of 6 Bft gusting to 8 Bft in showers were reported when probing work ended late that evening.

The low was forecast to move past the North Sea into the Skaw and then on into northern Scandinavia, so that the METEOR would experience northwesterly winds right into the North Sea, but diminishing to 4 Bft there and backing while the ship reached the Elbe estuary.

4.6 Station List

Table 4.3: CTD inventory

Station	Cast	Date 2001	Time UTC	Latitude North	Longitude West	m	Inst. Depth (m)
309	1	19/07	00:19	66° 20.54’	028° -02.26’	348	319
310	2	19/07	02:19	66° 13.86’	027° 31.25’	502	477
311	3	19/07	04:02	66° 11.86’	027° 22.22’	499	477
312	4	19/07	05:13	66° 09.97’	027° 13.74’	515	489
313	5	19/07	06:28	66° 07.91’	027° 04.91’	638	610
314	6	19/07	08:11	66° 03.52’	026° 46.89’	533	519
317	7	19/07	22:12	65° 59.98’	026° 30.41’	275	265
318	8	19/07	23:59	65 56.98	026° 14.84’	308	294
319	9	20/07	10:34	64° 52.84’	029° 59.92’	2062	2040
320	10	20/07	20:10	63° 34.67’	029° 59.56’	2173	2145
322	11	21/07	22:00	62° 33.10’	023° 45.77’	1314	1280
323	12	22/07	01:42	62° 10.04’	023° 16.11’	1466	1461
324	13	22/07	05:45	61° 45.89’	022° 46.15’	1746	1741
325	14	22/07	09:36	61° 21.97’	022° 29.59’	1861	1833
326	15	22/07	13:34	61° 00.92’	022° 09.10’	2040	2022
327	16	22/07	16:40	60° 46.90’	021° 51.02’	2296	2266
328	17	22/07	20:18	60° 27.19’	021° 39.62’	2560	2535
329	18	23/07	00:20	60° 11.91’	021 -15.02’	2719	2703
330	19	23/07	05:17	59° 43.11’	020° 54.81’	2834	2810
331	20	23/07	09:42	59° 19.97’	020 33.11’	2828	2817
332	21	23/07	14:21	58° 58.02’	020 11.93’	2828	2000
332	22	23/07	16:48	58° 58.06’	020 11.89’	2829	2805
333	23	23/07	21:13	58° 46.94’	020° 57.87’	2871	2847
334	24	24/07	02:32	59° 06.08’	021° 46.72’	2883	2887
335	25	24/07	07:40	59° 24.99’	022° 37.03’	2549	2525
336	26	24/07	12:38	59° 43.00’	023° 27.96’	2357	2352
337	27	24/07	17:22	60° 00.98’	024° 20.21’	2180	2150
338	28	24/07	21:52	60° 18.99’	025° 12.75’	2123	2202
339	29	25/07	02:36	60° 36.00’	026° 06.16’	2083	2092
340	30	25/07	07:14	60° 52.90’	027° 01.11’	1431	1403
341	31	25/07	10:54	61° 07.76’	027° 46.73’	842	834
342	32	25/07	16:15	60° 27.87’	028° 45.99’	1147	1128
343	33	25/07	22:27	59° 40.06’	029° 48.95’	1060	1067
344	34	26/07	20:38	59° 22.00’	028° 57.07’	1801	1799
345	35	26/07	07:19	59° 04.07’	028° 05.09’	2020	2000
346	36	26/07	12:22	58° 45.08’	027° 15.18‘	2231	2240
347	37	26/07	18:20	58° 27.00’	026° 24.96‘	2615	2589

Station	Cast	Date 2001	Time UTC	Latitude North	Longitude West	WD m	Inst. depth (m)
348	38	26/07	23:25	58° 06.99’	025° 36.13’	2711	2693
349	39	27/07	05:43	57° 48.07’	024° 47.94’	2806	2775
350	40	27/07	11:27	57° 32.01’	023° 59.99’	2903	2887
351	41	27/07	16:50	57° 14.04’	023° 09.96‘	3055	3035
352	42	28/07	08:47	56° 12.88‘	026° 37.05‘	2992	2969
353	43	28/07	19:23	55° 23.61‘	027° 56.50‘	2801	2773
354	44	29/07	10:40	54° 45.94‘	030° 25.10‘	2871	2844
355	45	29/07	21:16	53° 12.01‘	030° 04.97‘	3116	3095
356	46	30/07	03:56	52° 26.42‘	029° 50.19‘	3814	3792
357	47	30/07	08:52	52° 03.85‘	029° 40.26‘	3722	3709
358	48	30/07	15:55	51° 31.98‘	029° 58.04‘	3749	3728
359	49	30/07	23:43	50° 57.06‘	029° 57.66‘	3516	3508
360	50	31/07	06:19	51° 23.01‘	029° 54.90‘	3768	3530
361	51	31/07	12:28	51° 45.00‘	030° 00.96‘	3276	3325
362	52	31/07	20:50	51‘ 14.98‘	029° 59.57‘	3467	3520
363	53	01/08	04:18	51° 05.88‘	029° 57.95‘	4138	4109
365	54	01/08	18:14	50° 37.80‘	029° 42.92‘	3822	3840
366	55	02/08	05:37	48° 59.94‘	029° 43.06‘	3025	2986
367	56	02/08	20:16	46° 39.94‘	028° 14.96‘	3431	3420
368	57	03/08	02:21	46° 39.02‘	027° 21.04‘	3864	3827
369	58	03/08	07:58	46° 49.88‘	026° 33.92‘	2903	2791
370	59	03/08	12:19	46° 59.94‘	026° 01.94‘	3257	3252
371	60	03/08	17:25	47° 05.98‘	025° 16.90‘	3149	3127
372	61	03/08	22:20	47° 12.99‘	024° 33.04‘	3487	3488
373	62	04/08	06:59	47° 26.89‘	022° 56.98‘	4177	4176
374	63	04/08	15:57	47° 41.00‘	021° 20.91‘	4109	4087
375	64	05/08	00:37	47° 54.96‘	019° 43.95‘	4289	4378
376	65	05/08	09:18	48° 10.04‘	018° 06.89‘	4417	4438
377	66	05/08	15:00	48° 15.98‘	017° 20.86‘	4350	4369
378	67	05/08	21:22	48° 25.03‘	016° 23.84‘	4792	4822
379	68	06/08	04:14	48° 33.04‘	015° 26.93‘	4790	3010
379	69	06/08	06:43	48° 33.01‘	015° 26.98‘	4788	4818
380	70	06/08	13:54	48° 40.98‘	014° 30.00‘	4589	4603
381	71	06/08	19:35	48° 46.99‘	013° 47.12‘	4501	4528

Station	Cast	Date 2001	Time UTC	Latitude North	Longitude West	WD m	Inst. depth (m)
382	72	07/08	00:15	48° 50.14‘	013° 26.82‘	4427	4452
383	73	07/08	04:35	48° 52.94‘	013° 05.77‘	3650	3643
384	74	07/08	08:28	48° 56.04‘	012° 45.02‘	2036	2025
385	75	07/08	11:28	48° 59.06‘	012° 23.93‘	1341	1335
386	76	07/08	14:18	49° 02.04‘	012° 03.14‘	982	980
387	77	07/08	16:45	49° 05.05‘	011° 42.15‘	1129	1112
388	78	07/08	19:17	49° 07.99‘	011° 20.98‘	469	446
389	79	07/08	21:16	49° 10.90‘	011° 00.05‘	177	168
390	80	07/08	23:19	49° 13.98‘	010° 38.84‘	158	145

Table 4.4: Mooring Activities

Sta. No.	Int. No.	IfM No.	Date	Time	Latitude North	Longitude West	Depth (m)	Instr. Type	Remarks incl. nominal instr. depth
307			18/07	15:25	66° 11.59‘	027° 35.59‘	501		Test OFOS ok, Benthos release failed., 499m
307	SK	V423_2	18/07	20:50	66° 11.60‘	027° 35.50'	498	WH-ADCP	V423_2/SK/shield with ADCP 150kHz set ARGOS - WD-ID: Dec: 9243 Hex: 906C0
308	PIES006	V421_2	18/07	22:46	66° 14.00‘	027° 45.00‘	487	P/IES	V421_2/PIES006/shield set, 472m
315	LR	V425_2	19/07	11:09	66° 07.60‘	027° 16.20‘	582	LR-ADCP	V425_2/LR set, ADCP 75 kHz set ARGOS - WD-ID: Dec: 1176 Hex: 12618
316	PIES005	V422_2	19/07	12:44	66° 06.50‘	027° 10.50‘	625	P/IES	V422_2/PIES005 set, 610m
	TK		19/07	1930	66° 31.50‘	025° 26.00‘			fail to recover V424_1 because of ice coverage

Table 4.5: APEX- and RAFOS Float Launches

Sta. No.	CTD Cast	IfM No.	Date 2001	Time (UTC)	Latitude North	Longitude West	Argos (Dec.)	Argos (Hex.)	WMO tag	Cycle (days)	WRC S/N	Surface Temperature [°C]	Salinity	Remarks
APEX float launches ↓														
319	9	313	20/07	12:12	64° 53.10‘	030° 00.29‘	12624	C5404	6900157	10	0570	11.3	34.97	Irminger Basin
320	10	323	20/07	21:57	63° 34.63‘	029° 57.61‘	12626	C54A2	6900158	10	0571	10.9	34.96	Irminger Basin
327	16	311	22/07	18:19	60° 46.89‘	021° 51.00‘	12622	C53AC	6900155	10	0568	12.2	35.13	Iceland Basin “I“
346	36	312	26/07	14:11	58° 44.89‘	027° 14.94‘	12623	C53FF	6900156	10	0569	13.2	35.12	Iceland Basin “B“
350	40	310	27/07	13:44	57° 31.78‘	023° 59.65‘	12614	C5192	6900154	10	0567	14.0	35.05	Maury Channel “B“
354	44	326	29/07	12:39	54° 45.80‘	030° 25.18‘	12629	C5548	6900161	10	0574	13.4	33.93	Central Iceland Basin
365	54	324	01/08	20:57	50° 36.88‘	029° 43.80‘	12627	C54F1	6900159	10	0572	15.8	35.36	Mid Atlantic Ridge
367	56	325	02/08	22:52	46° 40.00‘	028° 15.04‘	12628	C55IB	6900160	10	0573	19.4	35.68	
373	72	308	04/08	09:57	47° 25.08‘	022° 57.74‘	07467	74AE1	6900152	10	0565	18.3	35.73	
379	69	309	06/08	10:01	48° 32.69‘	015° 26.94'	12611	C50DE	6900153	10	0566	18.1	35.61	
RAFOS float launches ↓										Mission (month)	SeaScan S/N	***Nominal Depth*** (m)		
325	014	534	22/07	11:14	61° 22.29‘	022° 29.58‘	5462	55599		14	RF # 49	1500		Reykjanes Ridge “I“
333	023	532	23/07	23:27	58° 46.99‘	020° 58.03‘	4989	4DF63		21	RF # 47	2600		Maury Channel
339	029	536	25/07	04:13	60° 36.07‘	025° 06.15‘	5467	556EB		12	RF # 51	1500		Reykjanes Ridge “A“
346	036	537	26/07	14:06	58° 44.89‘	027° 14.98‘	5481	55A6F		12	RF # 52	1500		Reykjanes Ridge “B“
349	039	533	27/07	07:37	57° 47.97‘	024°.47.56‘	5460	5553F		21	RF # 48	2600		deep Iceland Basin
353	043	535	28/07	21:34	55° 22.34‘	027° 57.04‘	5463	555CA		21	RF # 50	2600		deep Iceland Basin
355	45	538	29/07	23:40	53° 12.25‘	030° 05.03‘	5482	55A9A		21	RF # 53	2600		Near mooring “C“
357	47	539	30/07	11:38	52° 03.52‘	029° 39.76‘	5486	55B85		21	RF # 54	2600		Near mooring “Z“

4.7 Concluding Remarks

Leg 4 of METEOR cruise 50 served a multi-disciplinary team, all involved research questions of the North Atlanic. It is our common pleasure to thank *Kapitän* N. Jakobi and *Koordinator* F. Schott and their crews for excellent cooperation and assistance. Our Irish observer H. Cannaby was of great help in support of the CTD group on board. Funding of ship time and logistics was kindly provided by the *Deutsche Forschungsgemeinschaft.* All APEX floats deployed during M 50/4 were financed by a grand from the European Commission, Research Directorate-General (contract no. EVK2-CT-2000-00087 – GYROSCOPE).

4.8 References

Davis, R. and W. Zenk, 2001: Subsurface Lagrangian Observations during the 1990s. In: Siedler, G., Church, J., Gould, J. (Ed), Ocean Circulation and Climate, Academic Press, pp. 123-139.

Dickson, A.G., 1990. The oceanic carbon dioxide system: planning for quality data, JGOFS News, (2): 2.

Doe, 1994. Handbook of methods for the analysis of various parameters of the carbon dioxide system in seawater. ORNL/CDIAC-74, U. S. Dep. of Energy, Oak Ridge Natl. Lab., Oak Ridge, Tenn., USA.

Friis, K., 2001. Separation von anthropogenem CO_2 im Nordatlantik – Methodische Entwicklungen und Messungen. Dissertation. Christian-Albrechts-Universität zu Kiel, Kiel, 137 pp.

Grasshoff, K., Kremling, K. and Ehrhardt, M. (1999): Methods of seawater analysis. 3rd edition, Wiley-VCH, Weinheim.

Johnson, K.M., Wills, K.D., Butler, D.B., Johnson, W.K. and Wong, C.S., 1993. Coulometric total carbon dioxide analysis for marine studies: Maximizing the performance of an automated gas extraction system and coulometric detector. Mar. Chem., 44(2-4): 167-188.

Körtzinger, A., Thomas, H., Schneider, B., Gronau, N., Mintrop, L. and Duinker, J.C., 1996. At-sea intercomparison of two newly designed underway pCO2 systems - encouraging results. Mar. Chem., 52(2): 133-145.

Lewis, E. and Wallace, D.W.R., 1998. CO2SYS - Program developed for the CO2 system calculations. Carbon Dioxide Inf. Anal. Center; Report ORNL/CDIAC-105, Oak Ridge, Tenn., U.S.A.

Lorbacher, K, 2000: Niederfrequente Variabilität meridionaler Transporte in der Divergenzzone des nordatlantischen Subtropen- und Subpolarwirbels. Berichte des BSH , 22, 156 pp.

Millero, F.J., Byrne, R.H., Wanninkhof, R., Feely, R., Clayton, T., Murphy, P. and Lamb, M.F., 1993. The internal consistency of CO2 measurements in the Equatorial Pacific. Mar. Chem., 44(2-4): 269-280.

Mintrop, L., Perez, F.F., Gonzalez-Davila, M., Santana-Casiano, J.M. and Körtzinger, A., 2000. Alkalinity determination by potentiometry: intercalibration using three different methods. Ciencias Marinas, 26(1): 23-37.

Müller, T.J. 1999: Determination of salinity. In: Grasshoff, K., K. Kremling and M. Erhardt (Eds.): Methods of seawater analysis, 3rd edition, ch. 3, pp 41-73, Wiley-VCH, Weinheim.

Stephens, M.P., G. Samuels, D.B. Olson, R.A. Fine, 1995. Sea-air flux of CO_2 in the North Pacific using shipboard and satellite data. J. Geophys. Res. III, 100 (7): 13,571-13,583.

Takahashi, T., J. Olafsson, J.G. Goddard, D.W. Chipman, and S.C. Sutherland, 1993. Seasonal variation of CO_2 and nutrients in the high-latitude surface oceans: A comparative study. Global Biogeochem. Cycles, 7: 843-878.